ELSEVIER

Contents lists available at ScienceDirect

Powder Technology

journal homepage: www.journals.elsevier.com/powder-technology



On predicting the performance of different silicas on key property enhancements of fine APIs, blends, and tablets

Sangah S. Kim, Ameera Seetahal, Christopher Kossor, Rajesh N. Davé

New Jersey Center for Engineered Particulates, New Jersey Institute of Technology, Newark, NJ 07102, USA

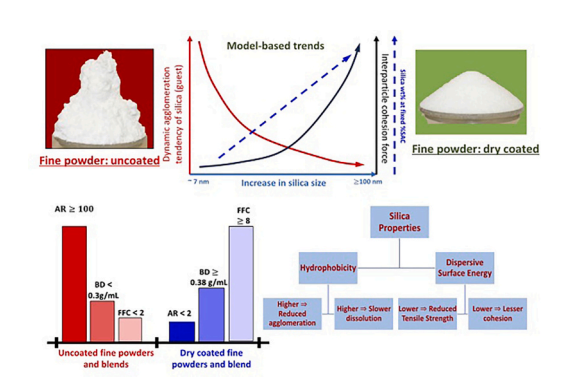
HIGHLIGHTS

- Studied predictive selection of silica size, amount, type (hydrophobic/ hydrophilic).
- Used multi-asperity, stick-bounce, guest-host suitability, & tablet hardness models.
- Assessed agglomeration, FFC, and BD of 4 APIs dry coated with 4 silicas at 2 SACs.
- Enhanced properties for APIs & mAPAP blends with all silicas; more for R972P & A200.
- Silica effect guided by various factors; its size a major driver; lesser the better.

ARTICLE INFO

Keywords:
Dry coating
Nano silica selection
Cohesive powder bulk property enhancements
Multi-asperity contact model
Surface energy
Tablet hardness

G R A P H I C A L A B S T R A C T



ABSTRACT

Predictive selection of silica size, type (hydrophobic/hydrophilic), and amount is addressed for achieving significant property enhancements of fine active pharmaceutical ingredients (APIs). Four models, Chen's multiasperity particle-adhesion, total surface energy-based guest-host compatibility, dispersive surface energy-based tablet tensile strength, and stick-bounce-based silica aggregation on coated particles, are invoked. The impact on the bulk properties of four APIs cohesive API powders ($\sim 10~\mu m$) and 40 wt% (wt%) blends of one API, dry-coated at 50% and 100% surface area coverage (SAC) of four nano-silicas (7–20 nm), hydrophobic (R972P), hydrophilic (M5P, A200, A300) is assessed. Significant enhancements in flowability, bulk density, compactability, agglomeration reduction, and dissolution for API or blend are achieved with all silicas. The experimental and model-based outcomes demonstrate that silica performance is impacted by multiple factors, silica size and coating effectiveness being most critical. In conclusion, R972P and A200 at lower 50% SAC present two excellent choices.

E-mail address: dave@njit.edu (R.N. Davé).

^{*} Corresponding author: Chemical and Materials Engineering, New Jersey Center for Engineered Particulates, New Jersey Institute of Technology, Newark, NJ, 07102, USA.

1. Introduction

Increased prevalence of micronized active powders in powder-based formulations [1-4] poses challenges for their handling and processing due to increased relative particle cohesion with reduced size [5-10]. Dry coating has emerged as an attractive environmentally benign approach [11,12] capable of fine powder cohesion reduction by an order of magnitude or more due to the resulting nano-scale roughness [11,13]. It has been shown to significantly improve powder flowability, bulk density, compressibility, and dispersibility [14-22]. Dry coating can be done through various high-intensity mixing devices such as the mechanofusion [16,20,21,23-25], hybridizer [26-28], theta-composer [29-32], Magnetically Assisted Impaction Coating (MAIC) [33], rotating fluidized bed coater [34], simultaneous milling and coating [35-37], conical mill [18,38,39], and a high-intensity vibratory mixer [19,40,41]. Previous studies have investigated various nanoparticles, e. g., metal oxides such as fumed silica, titania, alumina, etc. [17,31,35,42-50] or soft, wax-like spreadable materials, e.g., magnesium stearate (MgSt), leucine, etc. [25,51–57] as the dry coating (guest) particles to modify the surface properties of the cohesive (host) particles. More recently, a high-intensity vibratory coater, a.k.a., an acoustic mixer, has been reported to be a material sparing, lab-scale, and effective dry coating approach [58-60] utilizing various guest and host particle combinations. Significant bulk powder properties enhancements, including flowability, bulk density, compaction behavior, agglomerate reduction, and dissolution rate, have been reported for cohesive host powders dry coated with nano silica [61-66]. Collectively, these studies have provided insights into the impact of a few different types of silica on individual powders. However, the topic of judicious silica type selection while minimizing the silica amount and its subsequent impact on blend properties where one constituent is dry coated with a specific silica has not been well-explored. Further research in this aspect is warranted to minimize exposure due to the potential increase in cytotoxicity as silica size decreases and based on FDA recommendations. The well-established industry guidelines to handle silica and most pharmaceutical compounds include wearing personal protective equipment for particulate handling, such as masks and goggles, while working with the lowest possible quantities in negative-pressured fume hoods [66-68].

The impact of silica size, amount, and the rationale behind its normalization based on the host particle size has been elegantly addressed in multi-asperity particle contact model, hereafter called Chen's model [13]. This model demonstrated that there exists an optimal guest particle size for the highest possible adhesion force reduction, which for cohesive host particles of \sim 5–100 μm is in the range \sim 5–25 nm. The model also provides theoretical basis for predicting the expected performance of silica; both in terms of the quantification of the level of cohesion reduction and the amount of silica, further discussed in Sections 2 and 3. Chen's paper [13] demonstrated that the highest cohesion reduction may be achieved through a certain amount of silica, equivalent to between 30% to no >100% theoretical surface area coverage (SAC) of a host particle's surface with nano silica (guest particle) [63,65,69,70]. Whereas Chen's model is deterministic and has a few simplifying assumptions such as uniformly distributed guest or nano-silica particles, Deng and Davé [71] employed a probabilistic approach and further emphasized the importance of SAC and resultant three possible contact regimes for dry coated powders, i.e., host-host, host-guest, and guest-guest. This model, called the Deng's probabilistic contact model, demonstrated smoother transitions between these three contacts, in terms of the SAC values, host-guest size ratio, and subsequent cohesion reduction. Nonetheless, both these models indicated that while SAC need not be very high, it should be adequate, e.g., 30% SAC, to achieve guest-guest contacts that provide maximal cohesion reduction, whereas the higher amounts are ill-advised. A few, recent papers have experimentally recognized that indeed less silica may be adequate and could also be beneficial in improving the blend

uniformity and flowability [70,72–74]. In fact, a recent paper considered over a dozen materials and demonstrated that the normalization of silica amount in terms of SAC is a better approach than the conventional fixed wt% approach [74]. Also, Kim et al. 2022a emphasized the importance of keeping SAC constant instead of employing a fixed wt% value [75]. In their work, both R972P and A200 were used. They found that A200 was more agglomerated on the surface of the host particles as compared to R972P at a fixed wt% dry coating, observed through SEM images [70]. Consequently, the cohesion reduction for A200 at fixed wt% for the dry coated host was less than fixed SAC, further highlighting the need to employ fixed SAC values instead of fixed silica wt%.

Chen's model [13] suggested that using smaller guest particles within the optimal range is preferable for achieving the maximum amount of cohesion reduction. However, recent work demonstrated that finer guest particles tend to have higher agglomeration tendency due to the use of high-intensity mixing devices typically used for dry coating [76]. Silica aggregation on the host particle surface negates the advantage of using finer silica, hence the silica selection may need to examine the aggregation tendency that may be predicted by the Zheng's stickbounce model [76]. In addition, one may need to examine the surface energy of guest and host particles to check their compatibility, introduced by Jallo et al. [77], and demonstrated in [69,75]. The host particle surface energy and its Log P values are phenomenologically identified critical factors may impact the bonding strength or tablet hardness [77,78] or surface hydrophobicity [65,79], restricting the type of silica that may be used. Etzler et al. demonstrated that the tablet tensile strength is proportional to the square-root of the dispersive component of particle surface energy [80]. Therefore, coating with silica with lower surface energy is likely to reduce the tablet tensile strength. All of these factors that may have different, and in some cases opposing, effects may be analyzed a priori using the available models. Hence there is a need for investigating the impact of the inherent physicochemical properties of host and guest particles for selecting the right type and amount of silica to achieve adequate bulk properties enhancements via a combined experimental and modeling study; the main topic of this paper.

Consequently, the predictions based on the following models were employed and described in the next section: (1) Chen's model for the selection of silica amount via normalization and corresponding cohesion reduction, (2) host-guest compatibility equation based on silica and API surface energy [69,75,77,81], (3) tablet hardness model relating dispersive surface energy with the tablet tensile strength [80], and (4) the stick-bounce model to assess the silica aggregation tendency [76]. Previous papers [72,75,82] have shown that both R972P and A200 are very effective hence they were included in this investigation. Two other hydrophilic silicas were included for offering additional choices to industry practitioners. Therefore, four different nano silicas were selected as the guest particles: three hydrophilic silicas of different sizes, M5P (20 nm), A200 (12 nm), A300 (7 nm), and one hydrophobic silica, R972P (18 nm). Four cohesive, similar-sized (d_{50} in range 10–15 μ m) but physiochemically different active pharmaceutical ingredients (APIs) were chosen as the hosts: micronized acetaminophen, micronized ibuprofen, micronized fenofibrate, and griseofulvin. Dry coating was performed for all guest-host pairs and the resulting products were tested to assess which guest material, i.e., silica, was the most effective for improving the host powder's properties such as the flowability, bulk density, and agglomeration at the same % SAC. One of the APIs, micronized acetaminophen, was selected as the model host powder to prepare blends at a fixed API concentration of 40 wt%. The rationale for its selection is discussed in the results section. These blends were tested for their bulk properties such as agglomeration, flowability, bulk density, tablet compactability, and API release rate to assess which of the four silicas performed well. This comprehensive investigation along with using different models for potentially predicting silica performance is expected to help provide guidelines to select the most suitable silica for achieving significant bulk property enhancements of individual dry

coated API powders and their blends.

2. Theorical models

2.1. Chen's model and normalization of silica amount

Rumpf [83] demonstrated the significant role of particle asperities in reducing short-range van der Waals force. This weak force dominates interparticle adhesion, without the presence of moisture and electric field, of the primary particle smaller than 30 μ m [5,9]. However, Rumpf's single asperity model cannot fully explain the reported phenomenon in the improvement of powder flow and bulk density due to cohesion reduction as the coverage of asperity (number of guest particles) vary [58,59,65,84]. The Chen's multi-asperity particle contact model [13] addressed this short-coming by employing geometric arguments that include the role of SAC expressed in Eq. (1).

$$F_{\text{ad}} = \frac{Ad}{4z_0^2} + \frac{A}{24\left(\sqrt{\left(1 + \frac{d}{D}\right)^2 - \left[\left(\frac{1.21}{\% \text{SAC}}\right)\left(\frac{d}{D}\right)\right]^2} - 1\right)^2 D}$$
(1)

Hamaker constant, A, is a function of host particle surface energy (see Eq. (2)), and % SAC represents the percentage of the theoretical surface area of the host particle covered by the guest particle (see Eq. (3)). The primary particle size (d_{50}) of host and guest (or asperity) were noted as D and d respectively. z_0 is the inter-atomic equilibrium separation distance between two particles, 0.4 nm.

$$A = 24\pi \left(\gamma_{\text{dispersive}}^2\right) D_0 \tag{2}$$

In above equation, $\gamma_{dispersive}$ and D_0 are dispersive surface energy of host particle and the atomic scale minimum separation distance at contact, 0.165 nm, respectively [75,85].

The three key assumptions made in calculating theoretical % SAC were: (1) non-deforming monodispersed perfect smooth spheres for both host (API) and guest (nano- silica) particles, (2) coating is discrete, and (3) coating is done based on the smallest number of guest particles, forming equidistance triangle [13]. Eq. (3), the theoretical % SAC, presented by Chen et al. 2008 [13] and Yang et al. 2005 [11], is shown below.

$$%SAC = \frac{N \times d^2}{4(d+D)^2} \times 100\%$$
(3)

Here, N is the number of guest particles covering 100% of theoretically available host particle's surface area. Rearranging Eq. (3) to calculate the weight percent of the guest particle (silica) required to have the target % SAC results in Eq. (4) [11,72,75].

$$wt\% = \%SAC \times \left(\frac{4 D^2 d \rho_d}{4 D^2 d \rho_d + D^3 \rho_D}\right)$$
 (4)

Here, ρ_D and ρ_d are the densities of the host and guest particles, respectively.

The computational and experimental analysis in the previous publications [13,25,58,59,65,75,86] provides the basis for selecting suitable SACs. Consequently, two cases of % SAC were selected to mimic potentially optimal (50% SAC) and complete (100% SAC) dry coating [70,75].

2.1.1. Relative particle cohesion: Granular Bond number, Bo_g

The granular Bond number, Bo_g , is the ratio of the inter-particle cohesion, e.g., van der Waals force, $F_{\rm ad}$, and the gravitational force, $F_{\rm mg}$, acting on a particle; see Eq. (5) below [9]. It has been known to have a direct correlation to the powder's bulk properties including flow, powder bulk density and agglomeration tendency [75,85,87,88]. Chen's model [13] was used to calculate $F_{\rm ad}$, followed by computing Bo_g of uncoated and dry coated (50% SAC) powders as per Eq. (5) below where

m is the mass of the particle and g is the gravity.

$$Bo_{g} = \frac{F_{ad}}{F_{\text{gravity}}} = \frac{F_{ad}}{mg} \tag{5}$$

2.2. Guest-host compatibility model: dry coating quality estimation

The guest-host compatibility model, which is based on a simple case of interactive mixture model [58,89] was adopted to calculate the spreading coefficient ($\lambda^{2/1}$) of the guest (particle 2) over the surface of the host (particle 1) and vice versa, assuming even and discrete distribution of the guests. The spreading coefficient can be calculated using below Eq. (6).

$$\lambda^{2/1} = 4 \left[\left(\frac{\gamma_1^1 \times \gamma_2^0}{\gamma_1^1 + \gamma_2^0} \right) + \left(\frac{\gamma_1^p \times \gamma_2^p}{\gamma_1^p + \gamma_2^p} \right) - \left(\frac{\gamma_2}{2} \right) \right]$$
 (6)

In the above equation, γ_1^d and γ_2^d are the dispersive surface energy particle 1 and particle 2. The polarity of particle 1 and particle 2 are denoted as γ_1^p and γ_2^p , respectively. γ_2 or γ_1 is the surface energy of particle 2 or 1. Jallo et., al. [77] considered a special case where the mixture is between two disparate sized powers and proposed that if the absolute difference between $\lambda^{2/1}$ and $\lambda^{1/2}$ is >5, preferably >10, good compatibility between the host and guest particles would be expected [58,69,75]. Coating quality estimation was performed for the model API and silica powders used for the current study to investigate if surface energy analysis based on Eq. (6) could explain the experimental observations for dry coated APIs.

2.3. Stick-bounce model: Guest particle agglomeration tendency

Zheng's stick-bounce model [76] assumes two frictionless, perfect half spherical solid particles in head-on contact where they either collide and bounce off or collide and stick together, for which the model relied on Hertz and JKR contact equations. It is noted that as discussed in a recent study by Chen et al. 2023 [90], both Hertz and JKR models could lead to large deviations in the contact geometry, thus, the contact radius, force, and time. Nonetheless, these assumptions are reasonable for the purpose of qualitatively assessing the relative agglomeration tendency of different guest particles.

Zheng's stick-bounce model allowed estimating guest particles aggregation tendency, $K_{\rm d}$, for a high intensity LabRAM dry coating process (operated at 75G, 60 Hz) as a function of primary particle radius (r), particle material density (ρ) , surface energy (λ) , Poisson's ratio (υ) , and Young's modulus (E) of both host (API particle) and guest (nano silica) particles. $K_{\rm d}$ is the ratio between the energy required for deagglomeration (DA) and the kinetic energy supplied for agglomerate detachment (KE). The first order assumption between a pair of guest particles was used for the sake of simplicity to estimate DA which can be summarized as shown in Eq. (10). The graphical representation of the stick bounce model is presented in Fig. 1.

Consider reduced radius (R^*) and elasticity (E^*) given as follows.

$$\frac{1}{R^*} = \frac{1}{r_h} + \frac{1}{r_g} \tag{7}$$

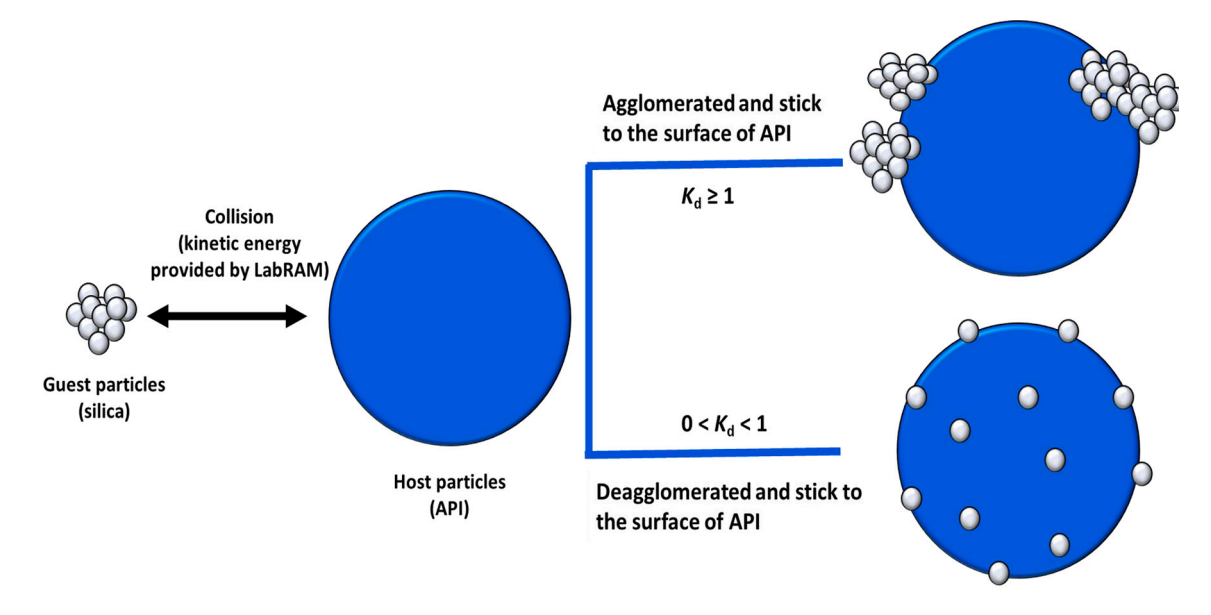
$$\frac{1}{E^*} = \frac{1 - \nu_h^2}{E_h} + \frac{1 - \nu_g^2}{E_g}$$
 (8)

Hertz contact theory gives the contact radius, a as

$$a = \sqrt[3]{\frac{3R^*}{4E^*}F} \tag{9}$$

In the above, r_h , r_g , E_h , E_g , v_h , and v_g are radius of host and guest, Young's modulus of host and guest, Poisson's ratio of host and guest, respectively. F shown in Eq. (9) is estimated contact force between guest and host particles.

Thus, Zheng's stick-bounce model equation can be expressed as the



 $K_d = f$ (Guest-host contact radius, guest & host van der Waals force, material stiffness, kinetic energy)

Fig. 1. Graphical representation of the stick-bounce model.

following.

DA = Plastic deformation energy + van der Waals energ =

$$\frac{A a^2}{12D_0^2} + \frac{A r_{\rm g}}{12D_0} + \frac{F a^2}{r_{\rm g}} \tag{10}$$

In the above, A and D_0 are the Hamaker constant and minimum separation distant at contact (see Eq. (2)). The contact force, F can be estimated using Eq. (11). E_h , E_g , v_h , v_g , r_h , r_g are Young's modulus of host, Young's modulus of guest, Poisson's ratio of host, Poisson's ratio of guest, radius of host, radius of guest, respectively.

$$F = \frac{\widehat{m} \triangle \nu}{t} \tag{11}$$

In the above, \hat{m} is the relative mass calculated using Eq. (12), Δv is the relative velocity change before and after the collision. The collision time, t, is calculated using Eq. (13) [91].

$$\widehat{m} = \frac{m_{\rm h} m_{\rm g}}{m_{\rm h} + m_{\rm g}} \tag{12}$$

$$t \approx 2.86 \left[\frac{\widehat{m}^2 E^{*2}}{\frac{r_h r_g}{r_h + r_g} \nu} \right]^{1/5} \tag{13}$$

Kinetic energy, KE, is estimated using Eq. (14).

$$KE = \frac{1}{2}\widehat{m}\nu^2 \tag{14}$$

2.4. Tablet tensile strength model accounting for the effect of dispersive surface energy

The Ryshkewitch and Duckworth equation presented below illustrated the empirical relationship between the tablet porosity and tensile strength at different compaction pressures.

$$\tau = \tau_0 e^{-k\varepsilon} \tag{15}$$

In the above equation, τ , τ_0 , k, ε are tensile strength of tablet, tensile strength of tablet at zero porosity, characteristic constant, and tablet porosity, respectively. Unfortunately, Eq. (15) does not explicitly

capture the effect of surface energy that drives the bonding strength between the powder materials. A general approach discussed by Etzler et al. [80], brings the effect of the dispersive surface energy shown in Eq. (16) below.

$$\tau \propto \gamma = \left(\gamma^{1/2}\right)^2 \tag{16}$$

Eq. (16) describes the contact between the identical particles, where γ is the surface energy.

Eqs. (15) and (16) were combined as below by Etzler for multicomponent blends of similarly sized constituents.

$$ln(\tau) = \sum_{i} \varphi_{Vi}[ln(\tau_{0i}) - k_{i}\varepsilon]$$
(17)

Eq. (17) accounts for volume fraction (φ_{Vi}) of each component.

3. Materials and methods

3.1. Materials

Fenofibrate (FNB, Jai Radhe Sales, Ahmedabad, India), ibuprofen (Ibu, generously gifted by BASF, USA), griseofulvin (GF, Hegno, China), and micronized acetaminophen (mAPAP, generously gifted by Mallinckrodt Inc., USA) were the selected four model APIs. The as-received Ibu and FNB (d_{50} of ~70 µm and ~ 40 µm, respectively) were micronized to a finer size ($d_{50}\sim15~\mu m$). Microcrystalline cellulose (Avicel PH105, gift from FMC Biopolymer, USA) was used as a filler, and lactose (Pharmatose 450, gift from DFE, USA) was added as a binder to mimic a commercial tablet powder blend. Magnesium stearate (MgSt, Mallinckrodt Inc., USA) was used as a lubricant for easier tableting. The current study did not include a disintegrant for the purpose of maximizing sensitivity between the dry coating formulation on the API release rate from the tablets. Aerosil A300 (nano-sized hydrophilic silica), Aerosil A200 (nano-sized hydrophilic silica), Aerosil R972P (nanosized hydrophobic silica), all generously gifted by Evonik Corporation (Piscataway, NJ, USA), and Cab-O-sil M5P (gifted from Cabot Corporation (MA, USA)) were chosen as the dry coating materials [75,92]. The properties of the materials are presented in Table 1. The log P values of APIs in Table 1 were taken from the references [65, 93, 94].

Table 1Properties of the APIs, excipients, and four silicas.

Materials	Mean particle size at 1.0 bar dispersion (μm)	Particle density (g/ mL)	Log P value of APIs [58, 64, 65]
Micronized acetaminophen (mAPAP)	8.3 ± 0.2	1.29 ± 0.02	0.49
Milled ibuprofen (mIbu)	$14.0\ \pm0.2$	$1.14{\pm}\ 0.01$	3.9
Milled fenofibrate (mFNB)	6.9 ± 0.0	1.25 ± 0.01	5.24
Griseofulvin (GF)	9.1 ± 0.3	1.51 ± 0.02	2.18
Avicel PH105	18.9 ± 0.1	1.43 ± 0.01	
Pharmatose 450	19.5 ± 1.7	1.48 ± 0.01	
MgSt	7.7 ± 0.2	1.01 ± 0.01	
R972P (Hydrophobic nano fumed silica)	0.018	2.65	
M5P (Hydrophilic nano fumed silica)	0.020	2.45	
A200 (Hydrophilic nano fumed silica)	0.012	2.45	
A300 (Hydrophilic nano fumed silica)	0.007	2.45	

3.2. Methods

3.2.1. Micronization by milling APIs

A fluidized energy mill (FEM) (Pharmaceutical Micronizer Fluidized Energy Grinding Jet mill, Sturtevant Inc., Hanover, Massachusetts) was used to produce micronized Ibu (mIbu) and fenofibrate (mFNB). The FEM powder feeding rate, feeding pressure, and grinding pressure were varied as per previous papers to achieve the desired final milled sizes [75,92,95].

3.2.2. Qualitative particle morphology analysis: Scanning Electron Microscopy (SEM)

Qualitative dry coating effectiveness was studied using a Scanning Electron Microscopy (SEM, EM JSM-7900F, JEOUL USA) [70,75]. Details of sample preparation for SEM imaging may be found elsewhere [65].

3.2.3. Dry coating method

A material sparing, high-intensity vibratory mixer (LabRAM, Resodyn, USA) was used as the dry coating device [59,96]. The amount of silica required for a given weight of the API powders (\sim 66% by volume of a standard 300 mL screw-top plastic container, equivalent to 30 to 40 g) was calculated based on the theoretical estimates of the surface areas of the host (API particle) and the guest (nano silica), as shown in the above Eq. (4) [11,72,75]. The container was filled with \sim 40 g of the API powders with the computed amount of nano silica and mixed in the

LabRAM for 5 min at 75 times the gravitation force at 60 Hz. The corresponding dry coating formulation is presented in Table 2, which also includes corresponding % SAC values for 1 wt% fixed dry coating for reference.

3.2.4. Powder true density measurements

A helium multipycnometer (P/N 02029–1, Quantachrome Instruments, USA) was used to measure an individual powder's true particle density. For each case, ten repeated measurements were taken under a helium environment to ensure repeatability. Assuming that the blends are ideal mixtures, the particle densities of all prepared blends were calculated using the following equation [97,98].

$$\rho_{\text{blend}} = \sum_{i=1}^{N} x_i \rho_i \tag{18}$$

In the above, each x_i and ρ_i denotes the mass fraction of component i and particle density of component i, respectively.

3.2.5. Particle surface energy measurements

A particle's total surface energy, the sum of the Liftshitz-van der Waals dispersive surface energy and the polarity, was evaluated using an automated inverse gas chromatography (SEA-IGC; Surface Energy Measurement Systems Ltd., UK). The details of sample preparation and analysis methods may be found elsewhere [69,99]. The measured surface energy of the API particles before dry coating was used to estimate the comparability between the selected API and each silica type.

3.2.6. Particle sizing: primary and agglomerated size evaluation

Two different particle sizing methods were utilized to measure primary and agglomerated particle size distribution with and without dry coating the APIs and blends. Primary particle size was measured via compressed dry air dispersion using the Rodos unit along with Helos laser diffraction particle sizer (Rodos/Helos, Sympatec, USA). The Rodos dispersion was done at 1 bar, selected based on pressure titration, details may be found in the previous papers [65,70]. Even the lowest dispersion pressure (0.1 bar), there was no discernment of natural state of API agglomeration for all APIs with or without dry coating [65,70]. However, the Rodos/Helos system provided very reliable sizes for the primary particles at 1 bar dispersion pressure. For a more accurate assessment of the natural agglomerate sizes, a gentler gravity dispersion based (Gradis) dynamic imaging (QicPic) particle sizer (Gradis/QicPic, Sympatec, USA) was used as per the detailed investigation reported in the previous studies [65,70,100–103].

Both particle sizers are highly reliable by providing repeatable measurements, requiring a minute sample for replicate measurements. The measured particle size distribution (PSD) data for the Rodos/Helos was consistent due to the effective particle dispersion requiring only a triplicate repetition per sample. However, a minimum of ten repetitions

Table 2Dry coating formulation for the APIs for each silica at two different theoretical surface area coverages (100% and 50% SAC).

100%		(corresponding wt%	% of silica)		50% SAC (corresponding wt% of silica)			
Silica API	M5P	A200	A300	R972P	М5Р	A200	A300	R972P
mAPAP	2.78	1.68	0.98	3.00	1.39	0.84	0.49	1.50
mIbu	2.17	2.07	0.77	3.68	1.08	1.03	0.38	1.84
mFNB	3.57	2.25	1.27	4.00	1.79	1.13	0.64	2.00
GF	2.08	1.26	0.74	2.25	1.04	0.63	0.37	1.13
Corresponding %		1 wt% fixed silica v ling %SAC at 1 wt%	· ·					
	M5P	A200	A300	R972P				
mAPAP	36.0	59.5	102.0	33.3				
mIbu	46.1	48.3	129.9	27.2				
mFNB	27.0	46.2	78.7	31.0				
GF	48.1	79.4	135.1	44.4				

per sample (total usage per sample is less than \sim 3 g) were performed for the Gradis/QicPic system to ensure the reproducibility and statistically meaningful averaging of the results for agglomerate PSD assessment.

The agglomerate ratio (AR), a dimensionless size ratio between the d_{50} of agglomerated particle size and the d_{50} of primary particle size, was used to quantify the degree of particle agglomeration with and without dry coating. The agglomerated particle size measurement value was taken from the gravity-dispersed dynamic imaging particle sizer, and the primary particle size measurement value was taken from the compressed air dispersion-based laser diffraction particle sizer.

$$AR = \frac{d_{50,Agglomerated (Gradis)}}{d_{50,Primarv (Rodos)}}$$
(19)

3.2.7. Bulk flow and density assessments

A FT4 powder rheometer (FT4, Freeman Technology, UK) was used to evaluate bulk powder flowability, bulk cohesion, and bulk density of an individual host powder and blends with and without dry coating, following previously reported procedure [65,72]. Two acrylic cylinders of 25 mL \times 25 mm and 10 mL \times 25 mm were used for bulk powder density measurement, bulk cohesion, and flowability assessments, respectively. A pre-shear normal stress of 3 kPa was applied throughout all relevant assessments. Flow Function Coefficient, FFC, the ratio between the major principal stress and unconfined yield strength [104] was used to quantify the powder flowability. The numeric value can be used to classified flow regimes: no flow (0 \times FFC \times 1), very cohesive (1 \times FFC \times 2), cohesive (2 \times FFC \times 4), easy-flow (4 \times FFC \times 10), and freeflow (10 \times FFC) [105]. Triplicate of bulk density assessments was done per sample whereas six to ten repeated measurements were done for bulk cohesion and flowability evaluation to confirm the repeatability.

3.2.8. Blend preparation: low-intensity mixing using a V-blender

The most cohesive API out of the four available selections, mAPAP, was selected to prepare cohesive and fine particle-sized blends comprised of 40 wt% of mAPAP, equal parts of Avicel PH 105 and Pharmatose 450 (for example, 29.5 wt% each for uncoated mAPAP blend) and 1 wt% of MgSt; see Table 3. Mixing parameters, including a V-blender container size of 600 mL and its volume fill-level, mixing intensity, and mixing time, were held constant for all blends to prevent any confounding effects [106,107]. The same protocol for charging or addition of the powder constituents in the blender was followed for all cases by pre-hand mixing all the constituents [108,109]. Hand-mixing involved adding the pre-weighted constituents (except MgSt) to a 1gal Ziplock plastic bag and gently shaking for ten seconds. The container fill level was kept at ~37% by volume (equivalent to 90 g of powder blends) for all cases. The total mixing time for each blend was fixed to ~16 min, equivalent to 500 revolutions with 25 rpm rotational speed, as per the outcomes from previous reports examining blend uniformity as a function of mixing time [63,72,73]. MgSt was added to the V-blender container during the last 90 s of mixing to avoid chances of over lubrication [63,99,110].

3.2.9. Tablet preparation: Gamlen D-series and Carver manual press

Tablets were prepared using two different methods. 70 mg (equivalent to 28 mg mAPAP dosage) tablets were prepared for tensile strength testing using Gamlen D-series tablet press (Gamlen Tableting Ltd., UK) with a 6 mm single punch die set [111]. Gamlen D-series press was used for this purpose due to its capability to use small quantities of powder per tablet (maximum $\sim\!\!150$ mg). That allowed obtaining a statistically significant number of samples (five to ten duplicates) per compaction pressure without the need for preparing excessive amount of dry coated API powders to be used for the blends.

Throughout tablet compaction, the hold time was kept constant at 5 s. 70 mg tablets were prepared by random powder sampling using a spinning riffler (SP-230, Gilson Company, INC., USA) [70,72]. The riffler has 16 collection ports with a test tube. A vibratory chute feeder tray fed the tubes while the riffler was spinning. After completion of the sampling of the entire bag, one test tube was randomly selected. That was followed by the next round of sampling on that tube, repeating until each subsequent sampling tube contained <100 mg of powders; see the details in [72].

Larger tablets were preferred for testing dissolution to reduce the influence from tablet weight variability of the API. A standard 12.7 mm die set with a flat-faced round punch and a manual Carver platen press (Carver, Inc., USA) were used to prepare 40 wt% mAPAP blend tablets under 155 MPa compaction pressure, for test of API release rate following USP <711> guidelines. Tablets, each at 200 mg where the sample collection procedure was as described in the above, were compacted at 155 MPa. This pressure was selected to obtain tablet strength of about 2.0 MPa, which was evaluated using a texture analyzer (Texture Technologies Corp., USA), testing five tablets per formulation.

Three tablets per formulation were tested for their moisture content with a thermogravimetric analyzer (TGA, TGA/DCS1/SF START^e system, Mettler Toledo Inc., USA) before testing the mAPAP release rate. Details of tablet preparation, tensile strength assessment with the texture analyzer, and TGA may be found elsewhere [70,95].

3.2.10. Tablet tensile strength assessment

The impact of guest selection and % SAC on tablet hardness was studied by varying compaction pressures from 240, 340, 470, and 600 kg, equivalent to 119.9, 169.8, 234.7, and 300.0 MPa. A diametrical compression test was done using the tablet tensile analyzer (TTA, Gamlen Tableting Ltd., UK) to evaluate tablet tensile strength for uncoated and dry coated 40 wt% mAPAP tablets. The tablet tensile strength was calculated by converting the tablet breaking force as per the following equation.

$$\sigma_{\rm T} = \frac{2 \times F}{\pi D_{\rm T} \delta_{\rm T}} \tag{20}$$

Here, σ_T , F, D_T , and δ_T represent the tensile strength of tablet, measured tablet breaking force, the diameter of the tablet, and thickness of the tablet, respectively. An automated digital thickness gauge (Mitutoyo, Japan) was used to measure the thickness of the tablets. A minimum of 10 tablets were tested and the calculated values were averaged.

Details of the mAPAP blend formulations.

	Uncoated	M5P		A200		A300		R972P		
	Control	100% SAC	50% SAC							
Constituent wt%	wt%	wt%	wt%	wt% wt%		wt%	wt%	wt%	wt%	
mAPAP	40	40	40	40	40	40	40	40	40	
Avicel PH105	29.5	28.94	29.22	29.16	29.33	29.30	29.40	28.90	29.20	
Pharmatose 450	29.5	28.94	29.22	29.16	29.33	29.30	29.40	28.90	29.20	
MgSt	1	1	1	1	1	1	1	1	1	
Colloidal silica	0	1.11	0.56	0.67	0.34	0.39	0.20	1.20	0.60	
Total wt%	100	100	100	100	100	100	100	100	100	

3.2.11. API release rate test using a USP II apparatus: 40 wt% mAPAP tablets

The release rates from the mAPAP tablets were tested via the USP II method (USP II, SOTAX, Switzerland) with 50 rpm rotating paddle and PBS pH 5.8 as the dissolution medium as per USP <711> guidelines. The system temperature was kept at 37 °C \pm 0.2 °C throughout the test. The solubility of acetaminophen in a PBS pH 5.8 buffer was measured to be \sim 15 mg/mL at the ambient condition [112]. Hence, 500 mL of pH 5.8 phosphate buffer was used as the dissolution medium throughout the testing, keeping the system in a sink condition. At the pre-determined time interval, 3 mL of samples were drawn. At each sampling, 3 mL of fresh make-up solvent was added, keeping the volume of the dissolution medium consistent. The dissolution samples were filtered with a 0.45 µm syringe filter, followed by dilution by adding 22 mL of the fresh dissolution medium to keep the API concentration within the UV-vis spectrometer (UV-vis spectrometer, Thermo Scientific, USA) detection range. The absorbance of the sample was measured in duplicate at the wavelength of 234 nm. At least three tablets per formulation were tested to check for repeatability in the mAPAP release rate trend.

Additionally, the wetting angle of the tablets was evaluated as supporting evidence using the sessile drop method [65,113,114]. The details of the method and results are discussed in the *Supplementary Materials* Section S1 for the sake of brevity.

4. Results and discussion

The weight amounts for each different silica for each API at two different % SAC values were estimated using Eqs. (3) and (4), presented in Table 2. For each fixed % SAC value, the largest-sized M5P silica requires three times the mass of the smallest-sized A300 silica because the wt% amounts are inversely proportional to silica sizes when they share identical particle densities. That suggests that if the finer silicas are equally effective at the same % SAC, it would be advantageous to use those since lesser amounts by mass or wt% is required. If the silica amounts were to be selected based on the fixed wt%, then the corresponding % SAC values for the 1 wt% fixed dry coating formulation are as presented in Table 2 [53,92,95,99]. The particle density difference, but most importantly, the size difference in the nano silica resulted in varying degrees of % SAC for fixed wt% despite the similarly sized host powders. For example, the % SAC values for mIbu ranged from 27.2 to 129.9, making it impossible to make a fair comparison of the performance of different silicas. Likewise, A300 as the guest resulted in % SAC >100 in several cases, which is undesirable. In contrast, R972P as the guest resulted in % SAC much lower in values (Table 2).

The ideal size of the silica has been addressed by the Chen model [13], which supports the selection of four popular, commercially available silicas that rather fortuitously fall in the desired size range of

~7-25 nm. This size range was also evident in the two previous experimental investigations [11,85]. For the sake of illustrating that silica higher sizes such as 50 nm or 100 nm are unsuitable, two hypothetical silicas of those sizes were considered in the computations of normalized particle cohesion or the granular Bond number, Bog, values. Those values were computed using Chen's model with experimentally measured dispersive surface energy (Table 4), particle true density (Table 1), and particle size (Table 5), all for the 50% SAC dry coated APIs. For the hypothetical 50 nm and 100 nm silicas, two different sets of surface energy values were taken from R972P and A200, respectively. The degree of cohesion reduction from dry coating was illustrated by plotting the normalized Bog with respect to the uncoated API in Fig. 2. Various cases are plotted in the order of increasing silica sizes. For all dry coated APIs, significant cohesion reduction is evident as expected. It is noted that the Bond numbers are plotted in a linear scale, whereas the bulk parameters such as the FFC are expected to be its power functions [74,75]. Therefore, Fig. 2 intentionally presents somewhat exaggerated differences for the influence of each type of silica and each API type. Nonetheless, based on this analysis, larger silica sizes are clearly not desirable, whereas one would expect A300 to be the most effective dry coating material out of four commercially available options. Consequently, A300 dry coated APIs are expected to show the most significant agglomeration reduction, highest bulk flowability and bulk density increases.

Interestingly, the experimentally measured bulk properties of the dry coated APIs did not match such predictions well, likely due to the higher agglomeration propensity of A300 compared to the other three commercially available silica as well as two larger hypothetical sized silicas as per the model-based predictions from Zheng et al. 2020 [76]. The agglomeration tendency evaluation with the stick-bounce model is summarized in Fig. 3, where the higher K_d values would indicate higher aggregation tendency. Since the Young's modulus values for the APIs are not readily available, very rough estimates are obtained in Fig. 3 by taking relatively low or high values for the Young's modulus of the API particles. The plotted results demonstrate rather weak sensitivity to the API's Young's modulus, and the results indicate that A300 having the highest K_d values would lead to the greatest aggregation of guest particles for all APIs. The trend of aggregation tendency in Fig. 3 is opposite that of Fig. 2, indicating these two different phenomena to be opposing each other and that using the smallest sized silica in the desired range may not be the best choice. Overall, one should not rely on the prediction of the silica performance solely based on the Chen model.

Table 4

Expected dry coating compatibility based on the surface energy measured at low (0.03n/m) IGC probe molecule coverage. The underlined values, which are greater than 10, indicate expected good compatibility.

Description	Hosts	Dispersive SE (mJ/ m2)	Polar SE (mJ/ m2)	Coated with R972P	Coated with M5P	Coated with A200	Coated with A300
	mAPAP	47.2	4.2	22.1	3.5	3.0	2.3
APIs, dry coated by silica (Direct dry coating)	mIbu	47.3	8.1	30.0	4.4	4.9	10.2
APIS, dry coated by silica (Direct dry couling)	mFNB	39.4	5.6	9.3	16.3	15.8	10.5
	GF	39.6	4.5	7.5	18.2	<u>17.7</u>	12.3
	MgSt	31.6	4.7	8.3	33.9	33.4	28.1
Excipients, contact with silica during blending	Avicel PH105	51.32	9.15	40.2	14.6	<u>15.0</u>	20.4
(no direct dry coating)	Pharmatose 450	41.6	6.5	<u>15.5</u>	10.2	9.7	4.4
	Guests	Dispersive SE (mJ/m2)	Polar SE (mJ/m2)				
	R972P	37.2	3.1				
Silica used for dry coating	M5P	41.0	12.2				
Silica used for dry coating	A200	42.8	10.2				
	A300	43.6	6.7				

Powder Technology 432 (2024) 119104

Table 5

Primary and agglomerated particle size distribution of uncoated and dry coated API. Primary particle sizing was repeated at least three times, while agglomerated particle sizing was repeated at the minimum of ten times per sample.

	Silica	API	Agglomerate PSD, Gradis			Primary PD	S, Rodos (1.0 b	ar)	Agglomerate ratio	
			d_{10}	d_{50}	d_{90}	Span $\left(\frac{d_{90}-d_{10}}{d_{50}}\right)_{\text{Gradis}}$	$\overline{d_{10}}$	d_{50}	d_{90}	$d_{50,\mathrm{Gradis}}/d_{50,\mathrm{Rodos}}$
	Uncoated	mAPAP	204 ± 63	1199 ± 382	2575 ± 653	2.0	2.5 ± 0.1	8.3 ± 0.2	25.0 ± 0.4	144 ± 0.3
		mIbu	$55.3 \!\pm 6.7$	$679 \pm\ 377$	1872 ± 489	2.7	3.8 ± 0.2	14.2 ± 0.2	33.3 ± 0.3	48 ± 0.6
		mFNB	51.9 ± 7.5	808 ± 254	2078 ± 540	2.5	2.8 ± 0.0	6.9 ± 0.0	14.7 ± 0.0	118 ± 0.3
		GF	$\textbf{87.4} \pm \textbf{7.6}$	271 ± 66	1543 ± 484	5.4	3.2 ± 0.1	9.1 ± 0.3	21.5 ± 0.7	30 ± 0.3
		mAPAP	20.9 ± 0.5	40.0 ± 2.6	314 ± 361	7.3	2.8 ± 0.0	9.7 ± 0.1	30.1 ± 0.3	4.1 ± 0.1
	M5P	mIbu	20.9 ± 0.2	34.9 ± 0.5	70.9 ± 6.1	1.4	4.9 ± 0.0	15.9 ± 0.1	36.1 ± 1.2	2.2 ± 0.0
	MSP	mFNB	20.9 ± 0.2	38.3 ± 0.7	89.1 ± 6.3	1.8	2.5 ± 0.0	$\textbf{7.4} \pm \textbf{0.0}$	23.4 ± 0.6	5.1 ± 0.0
		GF	61.4 ± 3.4	165 ± 19.2	539 ± 145	2.9	3.1 ± 0.1	$\textbf{9.4} \pm \textbf{0.2}$	24.7 ± 0.2	17.5 ± 0.1
		mAPAP	19.0 ± 0.4	35.8 ± 0.5	67.0 ± 4.0	1.3	2.7 ± 0.0	8.8 ± 0.0	26.2 ± 0.1	4.1 ± 0.2
	A200	mIbu	13.1 ± 0.1	25.1 ± 0.2	49.2 ± 4.0	1.4	2.9 ± 0.0	15.1 ± 0.1	29.4 ± 0.2	1.7 ± 0.0
	A200	mFNB	16.1 ± 0.9	29.7 ± 3.4	245 ± 271	7.7	2.8 ± 0.0	$6.6\pm~0.0$	15.4 ± 0.1	4.5 ± 0.1
1000/ 646		GF	16.1 ± 0.5	32.9 ± 2.3	173 ± 64.4	4.8	2.9 ± 0.1	8.6 ± 0.5	21.2 ± 0.2	3.8 ± 0.1
100% SAC		mAPAP	17.6 ± 0.4	32.9 ± 0.8	59.0 ± 3.5	1.3	2.6 ± 0.0	8.6 ± 0.1	25.5 ± 0.2	3.8 ± 0.3
		mIbu	23.0 ± 1.7	43.5 ± 9.1	992 ± 769	22.3	4.5 ± 0.3	15.7 ± 0.2	34.6 ± 0.4	2.8 ± 0.2
A300	mFNB	19.4 ± 0.3	34.7 ± 1.0	62.9 ± 2.8	1.3	2.2 ± 0.0	6.6 ± 0.1	15.9 ± 0.4	5.2 ± 0.1	
	GF	49.3 ± 4.2	130 ± 24.4	534 ± 364	3.7	2.9 ± 0.0	8.6 ± 0.1	20.9 ± 0.4	14.5 ± 0.1	
		mAPAP	16.0 ± 0.2	27.9 ± 0.4	42.0 ± 0.8	0.9	2.7 ± 0.0	8.7 ± 0.1	26.1 ± 0.4	3.2 ± 0.0
		mIbu	12.4 ± 0.2	22.8 ± 0.6	42.0 ± 1.7	1.3	2.8 ± 0.0	$15.2 \pm \! 0.0$	$31.7 \pm \! 0.0$	1.5 ± 0.0
	R972P	mFNB	17.3 ± 0.4	32.6 ± 2.2	477 ± 152	14.1	2.3 ± 0.0	6.4 ± 0.1	14.2 ± 0.3	5.1 ± 0.1
		GF	$15.8 \pm \! 1.3$	37.6 ± 13.8	580 ± 438	15.0	2.7 ± 0.7	8.1 ± 0.2	20.1 ± 0.1	4.6 ± 0.4
		mAPAP	17.6 ± 0.2	32.9 ± 0.8	96.1 ± 52.1	2.4	2.7 ± 0.0	8.9 ± 0.0	27.2 ± 0.2	3.7 ± 0.0
		mIbu	24.6 ± 0.4	40.6 ± 0.7	662 ± 378	15.7	4.7 ± 0.2	16.2 ± 0.1	36.5 ± 0.1	2.5 ± 0.0
	M5P	mFNB	19.5 ± 0.4	36.0 ± 1.0	75.1 ± 13.9	1.5	2.3 ± 0.1	7.0 ± 0.3	17.7 ± 0.9	5.2 ± 0.1
		GF	56.0 ± 5.2	146 ± 25.5	453 ± 75.1	2.7	3.1 ± 0.1	9.4 ± 0.4	23.5 ± 0.8	15.6 ± 0.2
		mAPAP	18.2 ± 0.3	34.9 ± 0.8	65.0 ± 2.7	1.3	2.6 ± 0.0	8.7 ± 0.1	25.7 ± 0.2	4.0 ± 0.0
		mIbu	16.2 ± 1.0	113 ± 168	1101 ± 323	9.6	2.8 ± 0.1	15.2 ± 0.2	30.6 ± 0.4	$\textbf{7.4} \pm \textbf{1.5}$
	A200	mFNB	16.5 ± 1.0	32.1 ± 6.6	349 ± 329	10.3	2.3 ± 0.0	6.4 ± 0.0	15.0 ± 0.1	5.0 ± 0.2
		GF	18.8 ± 1.6	42.7 ± 12.8	604 ± 378	13.7	3.0 ± 0.1	9.0 ± 0.5	21.6 ± 0.2	4.8 ± 0.4
50% SAC		mAPAP	17.8 ± 0.4	33.0 ± 0.7	59.5 ± 3.9	1.3	2.6 ± 0.0	8.6 ± 0.0	25.5 ± 0.1	3.9 ± 0.0
		mIbu	28.9 ± 1.1	50.2 ± 3.3	526 ± 455	9.9	4.7 ± 0.0	15.6 ± 0.1	35.3 ± 0.5	3.2 ± 0.1
	A300	mFNB	16.5 ± 1.0	32.1 ± 6.6	349 ± 329	4.2	2.2 ± 0.0	6.6 ± 0.1	15.9 ± 1.0	5.1 ± 0.0
		GF	80.1 ± 4.6	228 ± 25.9	732 ± 262	2.9	3.2 ± 0.0	9.6 ± 0.1	23.1 ± 0.4	23.8 ± 0.1
		mAPAP	15.8 ± 0.3	28.1 ± 0.6	44.6 ± 4.6	1.0	2.7 ± 0.0	8.7 ± 0.0	25.9 ± 0.1	3.2 ± 0.0
		mIbu	11.8 ± 0.1	22.4 ± 0.2	43.8 ± 1.9	1.4	2.8 ± 0.0	15.2 ± 0.0	31.7 ± 0.2	1.5 ± 0.0
	R972P	mFNB	15.0 ± 0.4	27.5 ± 0.7	181 ± 123	6.0	2.2 ± 0.0	6.0 ± 0.0	13.0 ± 0.1	4.6 ± 0.0
		GF	21.1 ± 2.1	67.4 ± 29.2	623 ± 378	8.9	2.9 ± 0.0	8.6 ± 0.1	20.9 ± 0.4	7.8 ± 0.5

4.1. Experimental results: Bulk properties of individual API powders

4.1.1. Individual API's agglomeration reduction with and without dry coating

The predicted normalized cohesion for dry coated APIs presented in Fig. 2 does not account for the potential issues with coating effectiveness due to surface energy mediated low compatibility between the host and guest particles that may be analyzed a priori through Eq. (7). Those computations for guest-host compatibility are presented in Table 4. These outcomes indicate that the hydrophobic R972P silica is more compatible with mAPAP and mIbu, whereas all three hydrophilic silicas are more compatible with mFNB and GF. Next, we examined if such predictions hold for how well these silicas may be dry coated. Consequently, powder samples of all dry coated APIs for each silica type and amount were examined for the silica coating effectiveness using an SEM. Typical image obtained are presented in Fig. 4, presenting uncoated and 50% SAC coated APIs. The corresponding 100% SAC coated APIs are shown in the Supplementary Materials, Fig. S1. These images qualitatively show that generally the dry coating of these silicas is effective and the differences amongst silica types are not significant. Although these observations are at the best highly qualitative, it appears that the use of high intensity dry coating device may have overcome guest-host compatibility issues evident in Table 4 for some cases. Nevertheless, closer examination reveals some differences such as: (a) For mAPAP and mIbu, hydrophobic R972P (Fig. 4(b) and (g)) seems to be better coated, partly in the sense that more of it is visible, than three hydrophilic silicas (Fig. 4(c), (d), (e) and (h), (i), and (k)); in line with the compatibility predictions in Table 4. (b) For mFNB, hydrophobic R972P (Fig. 4(l)) and

hydrophilic A200 (Fig. 4(n)) both seem to be well coated, indicating that their differing host-guest compatibility values of 9.5 and 15.8, respectively do not lead to striking differences in the coating quality. (c) While difficult to visualize due to its rough surface morphology, the coating is equal or better for the three hydrophilic silicas for GF as compared to hydrophobic R972P, also in line with the compatibility predictions in Table 4. (d) In most cases, there is aggregation of silica on host API surfaces, and it appears to be more for A300 even though lesser A300 is found on the surfaces as compared to other three silicas (Figs. 4(e), 4(j) and 4(o)).

Characteristic primary particle size and agglomerated particle size distribution of the uncoated and dry coated APIs are provided in Table 5 as per the procedure discussed in Section 3.2.6. Fig. 5(a) presents the normalized agglomerate size and the agglomerate ratio (AR), defined by Eq. (19), of the uncoated and dry-coated APIs. The most obvious trend for each model API is the significant agglomeration reduction due to dry coating, irrespective of the silica used. Interestingly, for all APIs, R972P (hydrophobic silica) was more effective as a guest particle in agglomeration size reduction than predicted by its poorer host-guest compatibility, Table 4, and the trends shown in Fig. 2. Further, there was no significant difference between 100% SAC and 50% SAC, at least for mAPAP and mFNB. In addition, surface energy measurements and spreading coefficient-based estimations indicated that mFNB and GF had better compatibility with hydrophilic silica (M5P, A200, and A300), hence lesser degree of agglomeration. However, that was generally not the case and could be attributed to high-intensity coating process whereas Eq. (7) is intended for conventional lower intensity mixers [75,115]. It is likely that the high energy intensity during dry coating

Powder Technology 432 (2024) 119104

Chen model prediction based Bog: 50%SAC cases

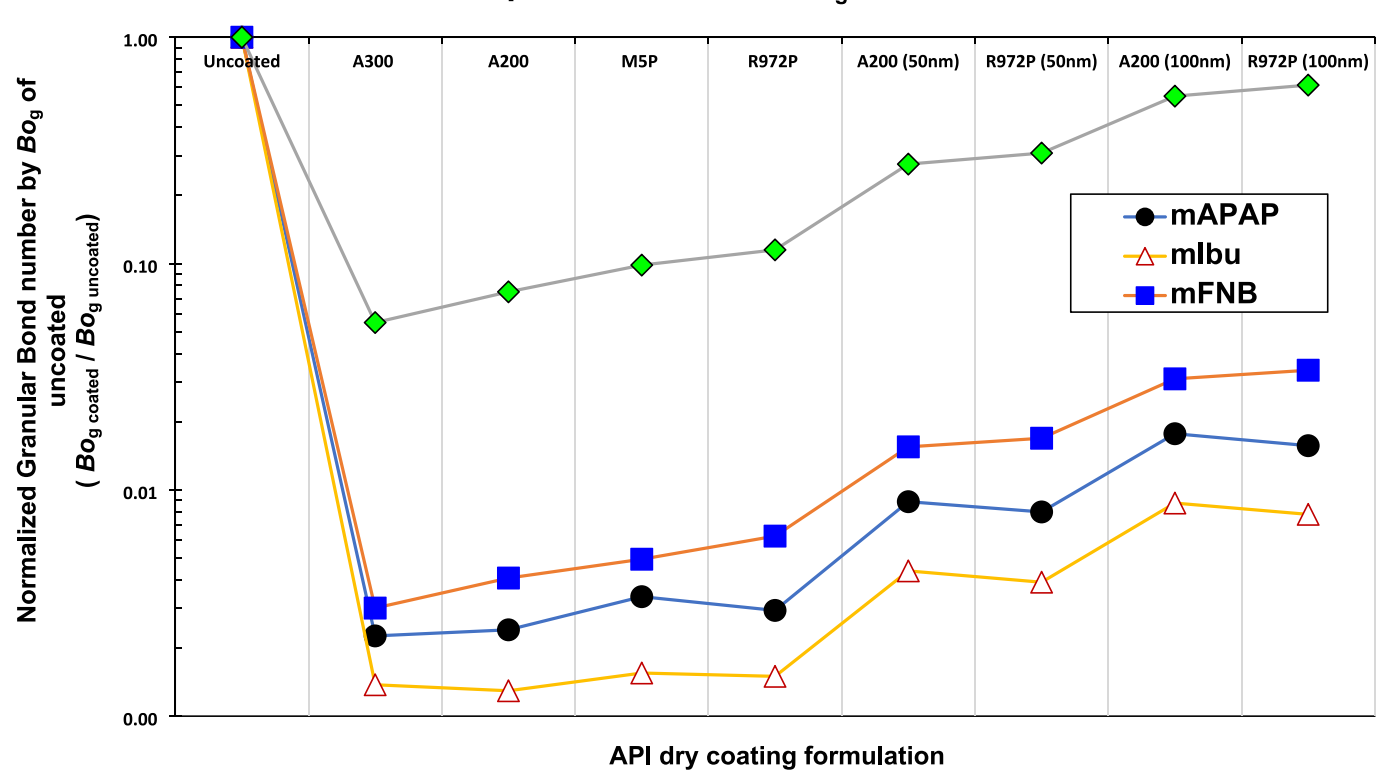


Fig. 2. Normalized particle cohesion expressed as the granular Bond numbers for the dry coated APIs at 50% SAC. These computations based on Eqs. (1) through (5) utilized experimentally measured surface energy, particle true density, and median particle size, all for the 50% SAC dry coated APIs.

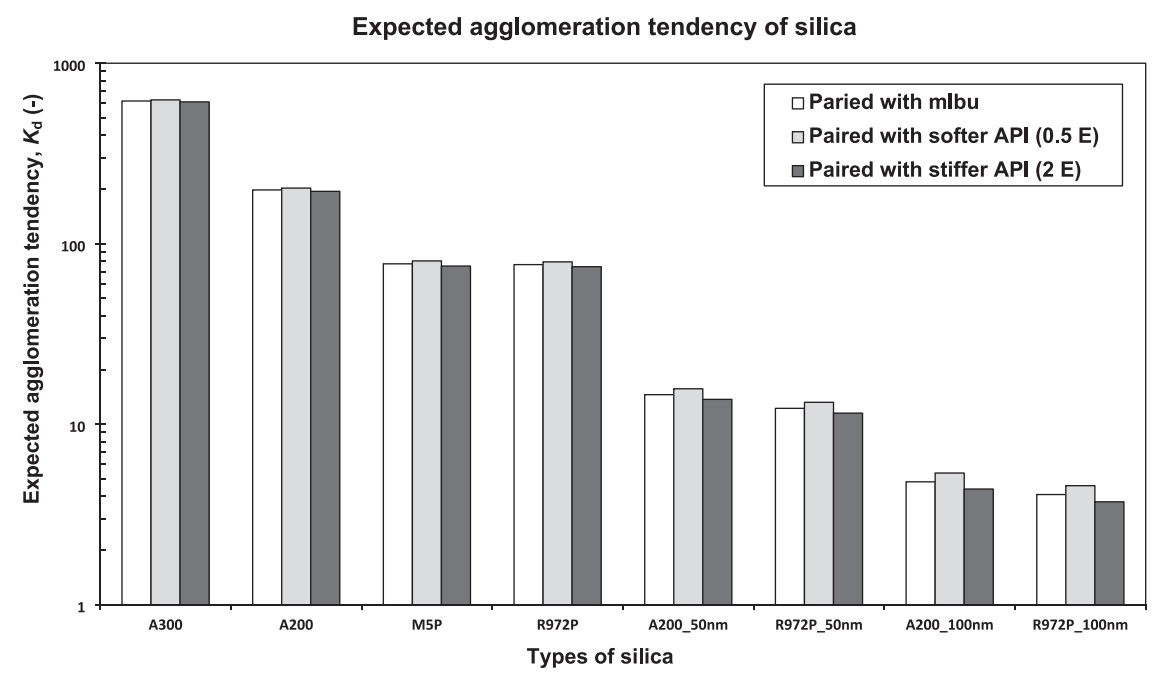


Fig. 3. Estimated aggregation tendency based on the stick-bounce model [76] for all four silicas. The values are computed for one high and one low value to the API Young's modulus, indicating low sensitivity and suggesting A300 to have the highest aggregation tendency amongst four silicas. Four additional cases with different-sized silica were added to demonstrate a significant impact of the guest particle size in its agglomeration tendency.

aided the spreading of guest particles on the surface of the host. Thus, the compatibility estimation using Eq. (7) [58] may only be applicable to low intensity mixing processes, more relevant to blend processing. Finally, lesser reduction in the agglomerate sizes for the hydrophilic

silica coated APIs could be attributed to the interaction between the hydrophilic silica and the available ambient moisture, potentially causing particles to agglomerate due to a capillary effect [116].

S.S. Kim et al. Powder Technology 432 (2024) 119104

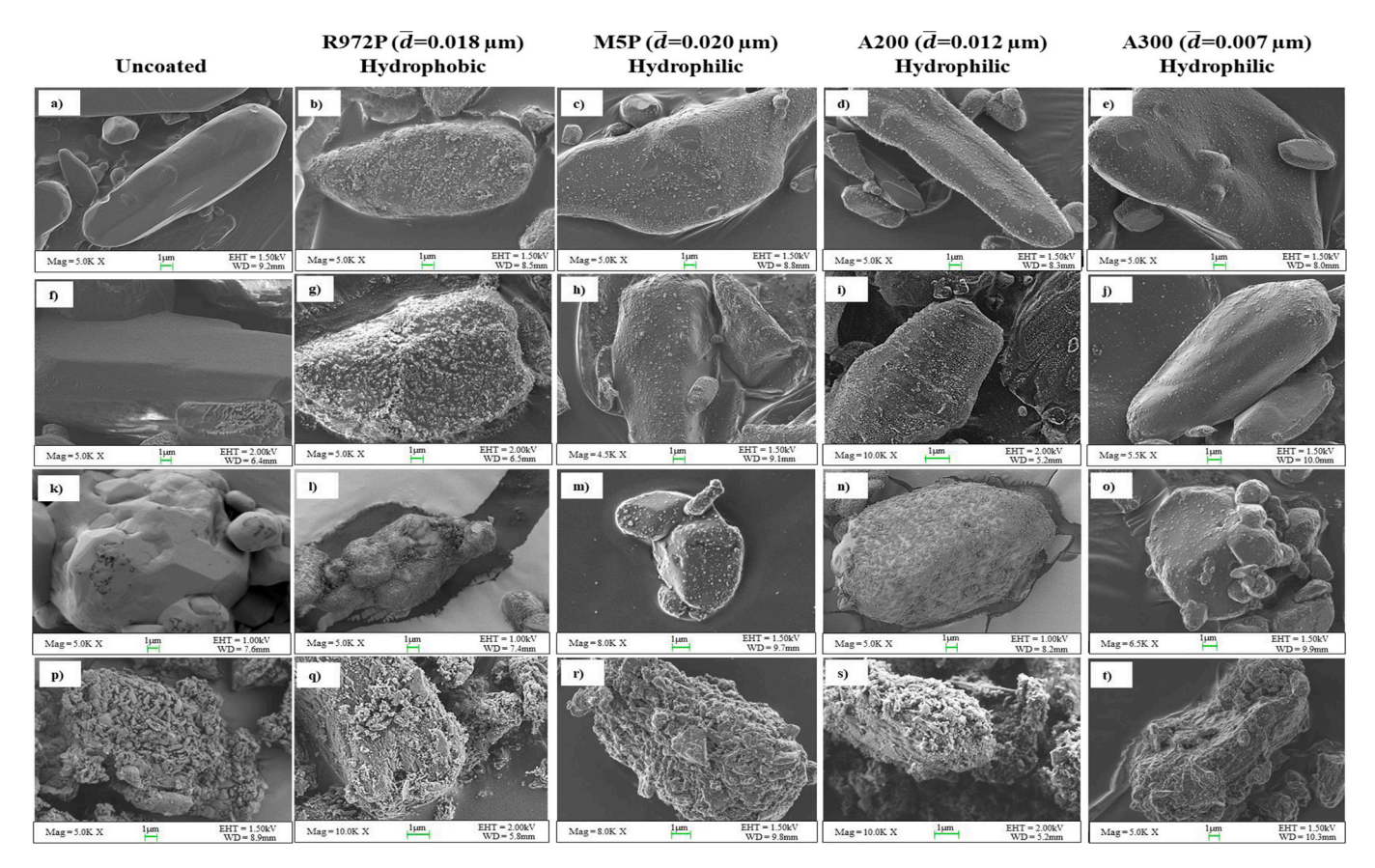


Fig. 4. SEM images of the exemplary APIs without and with dry coating (50% SAC) to qualitatively compare silica aggregation tendency: (a) \sim (e) uncoated and coated mAPAP; (f) \sim (j) uncoated and coated mIbu; (k) \sim (o) uncoated and coated mFNB; (p) \sim (f) uncoated and coated GF.

4.1.2. Flowability and bulk density of uncoated and dry coated APIs

The bulk properties of individual APIs with and without drying are presented in Table 6. The results for the powder flowability (FFC) and bulk density (BD) may be better visualized in Figs. 5(b) and 5(c), respectively. In general, dry coating enabled drastic API flowability improvement of up to three flow regimes, i.e., shifting from a very cohesive to a free-flowing range (Fig. 5(b)). The FFC results generally match the trend of the AR results (Fig. 5(a)), thus corroborating to the previously reported correlation between AR and FFC [75]. Similarly, the bulk density of the dry coated APIs had improved considerably, i.e., doubling in many cases, with an average of 50% increase for the uncoated API bulk density. Such dramatic flow property enhancements by all except GF, are in line with the reduced Bond number predicted by Chen's model (Fig. 2). GF is an exception is due to its macro-rough surface in its natural state [58,74,75].

4.2. Bulk properties of mAPAP blends

4.2.1. mAPAP blend's agglomeration reduction due to dry coating

Amongst four APIs, uncoated mAPAP had the highest cohesion (Table 6), lowest FFC and bulk density (Table 6, Figs. 5(b) and 5(c)), and highest agglomeration (Fig. 5(a)). It is also known to be a poorly compactible API [117,118]. Therefore, it was selected for the next level of experiments to test the influence of dry coating of the API on its blend agglomeration, flowability, bulk density, and compactability. Consequently, 40 wt% loaded blends of mAPAP were prepared with fine cohesive excipients (Avicel PH105 and Pharmatose 450). It is noted that while the selection of mAPAP is justified for these blend properties, it may not be best candidate for discerning the silica effect on drug dissolution from tablets, which was done for the sake of completeness. Nonetheless, previous work has considered ibuprofen for assessing the

dissolution affected by hydrophobic silica in detail [65,119]. It is noted that the cases of silica addition during blend mixing were not investigated because the previous studies have already reported far less effective blend properties improvements for the cases where nano silica was simply mixed in during blending instead of the dry coating of the APIs [69,70,72,120].

The assessment of the blend agglomeration with and without the API dry coating was performed and the AR values, evaluated as per Eq. (19), are presented in Fig. 6(a). Several observations are made: (1) The AR values for both uncoated and dry coated blends match closely with the AR values of the individual mAPAP. (2) Dry coating of mAPAP, which at 40% is a minority component of the multi-component blend, had a significant impact on the reduction of the AR values of all blends. (3) The AR reduction due to dry coating of mAPAP was nearly the same regardless of the type and amount of silica used for dry coating. The last observation for the blends is very interesting. That is because although the host-guest compatibility shown in Table 4 indicates performance differences for four silicas for individual API, i.e., mAPAP, it is in line with the higher compatibility predicted for all four silicas to the excipients (Avicel PH105, Pharmatose 450, and even MgSt) as compared with mAPAP. The reader may recall that the dry coating of mAPAP was done using a high-intensity mixer hence the Eq. (7) and results in Table 4 are not directly applicable. Therefore, the disagreement between the uniformly similar experimental AR values and the model predicted performance differences in Table 4 are justifiable. In contrast, the blend mixing was done using a conventional low-intensity mixer and the predicted results from Table 4 should hold, and the experimental results are indeed in line. That is because as per guest-host compatibility predictions, better silica re-distribution from mAPAP to excipients was expected, resulting in uniformly lower degree of agglomeration for blends than an individual API. In summary, dry coating of the API not

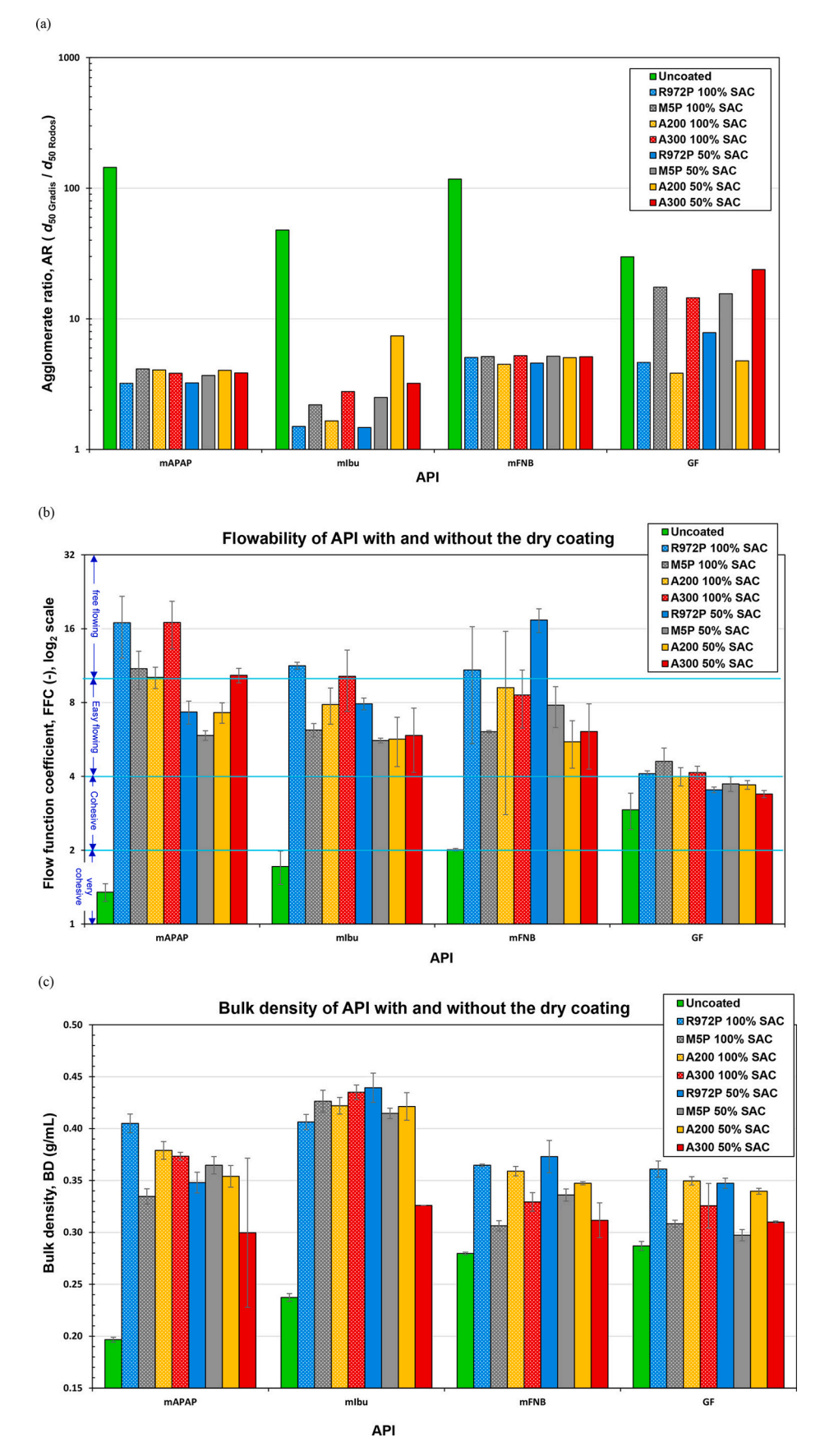


Fig. 5. Individual uncoated and different silica dry coated APIs bulk properties: (a) agglomerate ratio (AR, $d_{50 \text{ Gadis}} / d_{50 \text{ Rodos}}$), (b) bulk flowability (FFC), and (c) bulk density. To ensure reproducibility, a minimum of ten repeated measurements were taken for the agglomeration, and six repeated measurements were done to evaluate bulk flow and bulk density.

Table 6Bulk properties of APIs without and with dry coating. Each measurement was taken six times for the sake of reproducibility.

API	Dry coating	Bulk density BD (g/mL)	Cohesion (kPa)	Flowability FFC (–)
	Uncoated	0.20 ± 0.00	1.72 ± 0.23	1.35 ± 0.11
	R972P 100% SAC	0.41 ± 0.00	0.08 ± 0.01	16.91 ± 4.76
	M5P 100% SAC	0.33 ± 0.01	0.14 ± 0.03	11.00 ± 1.95
	A200 100% SAC	0.38 ± 0.01	0.15 ± 0.02	10.14 ± 1.01
mAPAP	A300 100% SAC	0.37 ± 0.01	0.11 ± 0.03	16.96 ± 3.74
	R972P 50% SAC	0.35 ± 0.00	0.21 ± 0.02	7.32 ± 0.79
	M5P 50% SAC	0.36 ± 0.01	0.30 ± 0.03	5.87 ± 0.26
	A200 50% SAC	0.35 ± 0.01	0.21 ± 0.03	$\textbf{7.28} \pm \textbf{0.70}$
	A300 50% SAC	0.30 ± 0.01	0.14 ± 0.01	10.33 ± 0.70
	Uncoated	$\textbf{0.24} \pm \textbf{0.00}$	0.90 ± 0.16	1.72 ± 0.27
	R972P 100% SAC	0.41 ± 0.01	0.19 ± 0.07	11.30 ± 0.38
	M5P 100% SAC	0.43 ± 0.01	0.23 ± 0.02	6.18 ± 0.39
	A200 100% SAC	0.42 ± 0.01	0.12 ± 0.07	7.85 ± 1.32
mIbu	A300 100% SAC	0.44 ± 0.01	0.15 ± 0.05	10.23 ± 2.87
	R972P 50% SAC	0.44 ± 0.01	0.23 ± 0.07	7.91 ± 0.44
	M5P 50% SAC	0.41 ± 0.00	0.25 ± 0.01	5.60 ± 0.13
	A200 50% SAC	0.42 ± 0.01	0.23 ± 0.08	5.68 ± 1.29
	A300 50% SAC	0.33 ± 0.01	$\textbf{0.26} \pm \textbf{0.09}$	5.87 ± 1.72
	Uncoated	0.28 ± 0.00	0.81 ± 0.02	2.01 ± 0.03
	R972P 100% SAC	0.36 ± 0.00	$\textbf{0.16} \pm \textbf{0.06}$	10.87 ± 5.43
	M5P 100% SAC	$\textbf{0.31} \pm \textbf{0.00}$	0.24 ± 0.01	6.08 ± 0.08
	A200 100% SAC	0.36 ± 0.00	0.21 ± 0.02	9.20 ± 6.41
mFNB	A300 100% SAC	$\textbf{0.33} \pm \textbf{0.00}$	0.22 ± 0.08	8.58 ± 2.28
	R972P 50% SAC	0.37 ± 0.02	$\textbf{0.08} \pm \textbf{0.01}$	17.36 ± 1.93
	M5P 50% SAC	$\textbf{0.34} \pm \textbf{0.01}$	0.18 ± 0.03	$\textbf{7.80} \pm \textbf{1.48}$
	A200 50% SAC	0.35 ± 0.00	0.27 ± 0.02	5.53 ± 1.21
	A300 50% SAC	0.31 ± 0.02	0.27 ± 0.03	6.10 ± 1.81
	Uncoated	0.29 ± 0.00	0.59 ± 0.14	2.92 ± 0.49
	R972P 100% SAC	0.36 ± 0.01	0.36 ± 0.01	$\textbf{4.10} \pm \textbf{0.11}$
	M5P 100% SAC	0.31 ± 0.00	0.33 ± 0.05	4.60 ± 0.62
	A200 100% SAC	0.35 ± 0.00	$\textbf{0.38} \pm \textbf{0.04}$	4.00 ± 0.34
GF	A300 100% SAC	0.33 ± 0.02	$\textbf{0.39} \pm \textbf{0.02}$	4.15 ± 0.25
	R972P 50% SAC	0.35 ± 0.00	$\textbf{0.44} \pm \textbf{0.02}$	3.53 ± 0.09
	M5P 50% SAC	0.30 ± 0.01	0.41 ± 0.04	$\textbf{3.73} \pm \textbf{0.25}$
	A200 50% SAC	0.34 ± 0.00	$\textbf{0.43} \pm \textbf{0.02}$	3.69 ± 0.15
	A300 50% SAC	0.31 ± 0.00	0.46 ± 0.02	3.39 ± 0.11

only significantly reduced the AR level of mAPAP, but also resulted in the reduction of the AR of its blends. Clearly, this could not be achieved if the silica was not dry coated and only added to the blend during conventional low-intensity mixing [69,70,72,120].

4.2.2. Flowability and bulk density of mAPAP blends

Next, the flowability and bulk density of the mAPAP blends are presented in Table 7. They are also presented in Figs. 6(b) and 6(c), respectively, for better visualization of the trends. Here, too, the impact of dry coating of the minority blend component, mAPAP, is evident. The FFC values, Fig. 6(b), for all 100% SAC mAPAP dry coating blends exceeded the level required for a direct blending and direct compaction (DB-DC) tableting [58,121] and ranged from just above 7.0 to over 21; the lowest being silica M5P. At lower amount of silica coating of 50% SAC, both A200 and A300 slightly underperformed, likely due to much lesser amount of silica being available for re-distribution. The results for the blend bulk density, Fig. 6(c), are similar to the FFC results, where six out of eight dry coating formulation cases achieved adequate values considered suitable for DB-DC tableting. Overall, in all cases, R972P dry coated mAPAP blends achieved the highest flow improvement to a level well above the requirement for DB-DC tableting. Considering that placebo FFC was measured at under 4.00 in the cohesive category and its Bulk density was below the DB-DC target (shown as a red horizontal line in Fig. 6(c), these are remarkable results for blend bulk density enhancements due to dry coating of a fine cohesive minority API component and are in line with the previous reports [70,72,73,119].

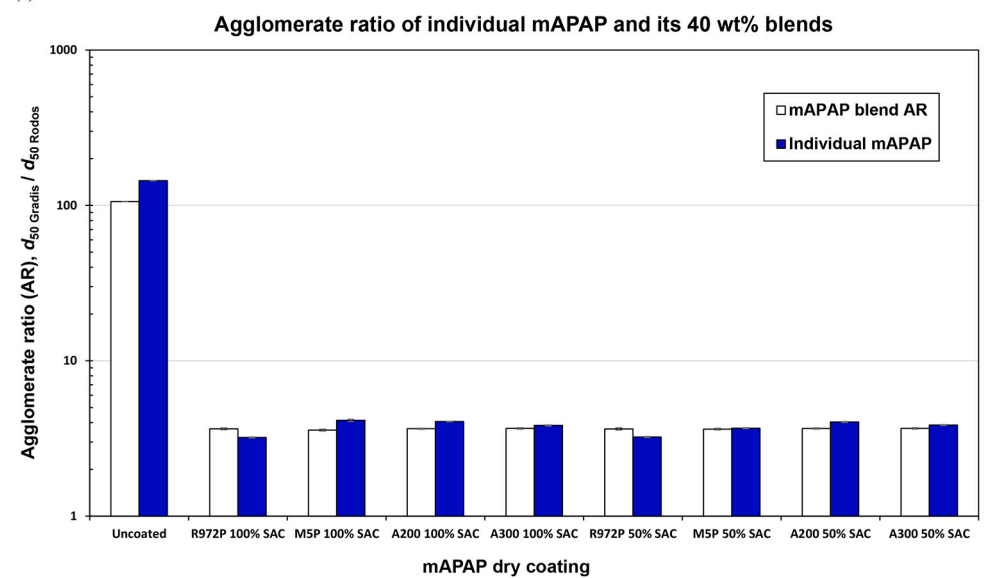
The flowability of blends is a crucial property attribute that affects tablet weight variability, hence, tablet product quality [122,123]. The USP <905> guideline recommends, especially for tablets with API dosage equal to or >25 mg, testing tablet-to-tablet weight variability as a key test to discern uniformity of tablets for medium to high API loading tablets [124]. Although tablet weight variability testing is outside the scope of this paper, the results of this work demonstrating significantly improved blend flowability, reduced agglomeration, as well as reduced API cohesion all suggest that one could expect improved API content uniformity [72,73] and lower tablet-to-tablet weight variability [125].

Next, the impact of using hydrophobic R972P silica, which was the most effective in cohesion reduction and correspondingly led to highest blend bulk properties improvements, on compactability of the tablets was tested since the hydrophobicity of R972P implying lower surface energy could lead to greater loss of the tablet tensile strength [126,127].

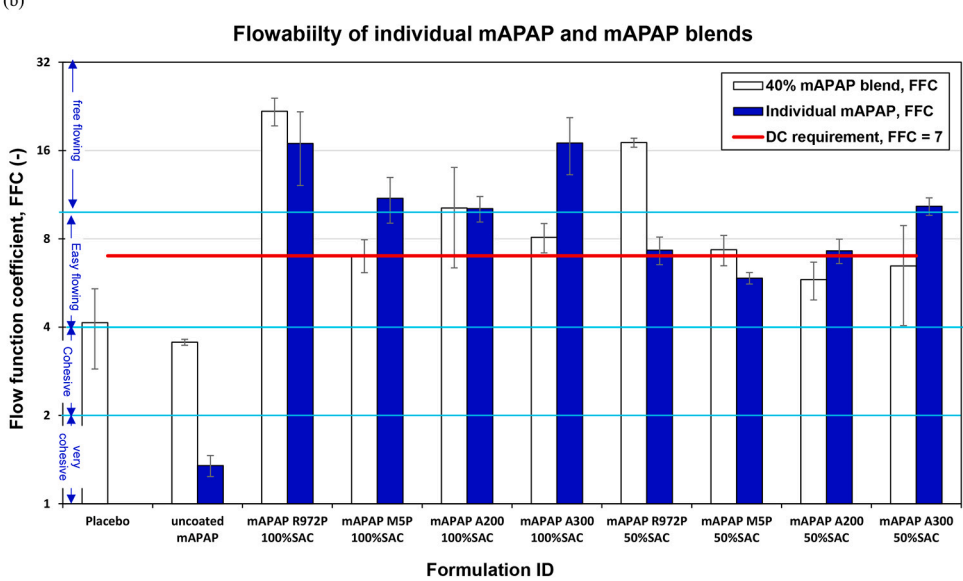
4.3. The blend tablet tensile strength: mAPAP dry coating with different silicas

Tablet hardness or tensile strength (TS), being a critical quality attribute [128], was assessed for each of the different dry coating formulations, at several compaction pressures of 240, 340, 470, and 600 kg (equivalent to 119.9, 169.8, 234.7, 300.0 MPa). The results for mAPAP dry coating at 50% SAC and 100% SAC, respectively, are presented in Figs. 7(a) and 7(b). The placebo TS values, presented for reference were the highest as expected because of poor compactability of mAPAP, and corresponded to their lowest tablet porosity (Supplementary Materials, Table S2) [96]. The horizontal lines at 2.0 MPa indicate the recommended TS for typical commercial oral tablets to prevent tablet breakage during transportation [59,63,121]. The results presented in Fig. 7 reveal a few trends, which although surprising, confirm previous work where the blends containing dry coated API did not exhibit any appreciable loss of TS. Although a tablet made of an individual dry coated powder may exhibit some loss of TS due to the presence of silica [59,119]. For lesser silica amounts (50% SAC, Fig. 7(a)), the tablet TS value at the lowest compaction pressure for the A200 coated mAPAP blend are the highest, and the M5P coated mAPAP blend are the lowest. At higher compaction pressures, the TS differences between R972P, A200, and A300 silicas coated mAPAP blends are minimal, comparable to the uncoated mAPAP blends, except for at the highest compaction force when the uncoated mAPAP blend has a lower TS. Such outcomes are rather surprising considering R972P has the lowest surface energy amongst these three silicas and uncoated mAPAP, since it is hydrophobic and its amount by wt% is the highest. This might be due to low agglomeration of powders due to R972P coating that could lead to easier

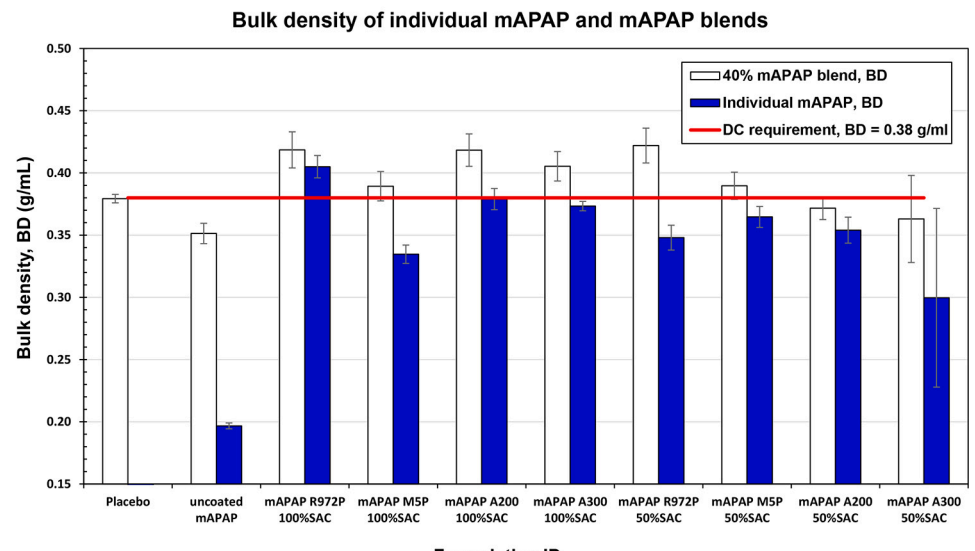
(a)



(b)



(c)



Formulation ID

Fig. 6. Properties of the different dry coated mAPAP blends containing 40 wt% API along with those of the mAPAP by itself in dak blue bars provided for reference: (a) blend agglomerate ratio (B-AR, $d_{50 \text{ Gadis}} / d_{50 \text{ Rodos}}$) of blends, (b) bulk flowability (FFC), and (c) bulk density (BD) of the blends. To ensure reproducibility, a minimum of ten repeated measurements were taken for the agglomeration, and six repeated measurements were done to evaluate bulk flow and bulk density. (For interpretation of the references to colour in this figure legend, the reader is referred to the web version of this article.)

Table 7Bulk properties of 40% mAPAP blends at different dry coating formulations. Each measurement was taken six times for the sake of reproducibility.

Blend description	Bulk density BD (g/mL)	Cohesion (kPa)	Flowability FFC (–)
Placebo	0.38 ± 0.00	$\textbf{0.38} \pm \textbf{0.06}$	$\textbf{4.14} \pm \textbf{1.26}$
uncoated mAPAP	0.35 ± 0.01	$\textbf{0.44} \pm \textbf{0.02}$	3.55 ± 0.08
mAPAP R972P 100% SAC	0.42 ± 0.01	0.07 ± 0.01	21.77 ± 2.35
mAPAP M5P 100% SAC	0.39 ± 0.01	0.22 ± 0.04	7.04 ± 0.91
mAPAP A200 100% SAC	0.42 ± 0.01	0.16 ± 0.06	10.19 ± 3.82
mAPAP A300 100% SAC	0.41 ± 0.01	0.20 ± 0.03	8.09 ± 0.93
mAPAP R972P 50% SAC	0.42 ± 0.01	0.08 ± 0.00	17.02 ± 0.60
mAPAP M5P 50% SAC	0.39 ± 0.01	0.21 ± 0.02	7.34 ± 0.87
mAPAP A200 50% SAC	0.37 ± 0.01	0.26 ± 0.04	5.81 ± 0.86
mAPAP A300 50% SAC	0.36 ± 0.04	0.25 ± 0.02	6.46 ± 2.42

particle rearrangement during pre-compaction, although further research may be necessary to better understand this outcome. The lowest TS value trend continues for the M5P coated blends at all compaction pressures and it is also surprising. The most noteworthy outcome is that for all four silicas, TS value of about 2 MPa was achieved at a compaction pressure of as low as $\sim\!235$ MPa, and for three of those, it was achieved at even lower $\sim\!170$ MPa compaction pressure.

For the higher 100% SAC silica levels, dry coating of mAPAP with A200 and A300 silicas resulted in even higher tablet TS values as compared to the uncoated mAPAP formulation, achieving >2 MPa at the compaction pressure of ~170 MPa or higher. Hydrophilic silica M5P was the least desirable choice even for these cases amongst four silicas from the tablet TS perspective, failing to achieve 2 MPa at any of the four compaction pressures for 100% SAC (Fig. 7(b)). This was surprising because although the tablet tensile strength should be proportional to powder material's total surface free energy (sum of dispersive and polar components) [80], it was the lowest for M5P having the highest surface free energy. Similarly, the higher amount of R972P at 100% SAC did not lead to lesser TS values as compared to those at 50% SAC, despite R972P being the one with the lowest surface free energy. Overall, these results demonstrate that R972P, A200, and A300 silicas, preferably in their lesser amounts (50% SAC), would have no adverse impact on tablet TS and may even provide harder tablets than those blend formulations that do not have any silica.

4.4. Dissolution testing of mAPAP tablets through USP II testing

As mentioned before, the use of a hydrophobic silica poses concerns regarding its adverse effect on drug dissolution from poorly water-soluble drugs. This topic was investigated previously where the effect of dry coating of micronized ibuprofen with R972P on drug dissolution from tablets indicated no adverse effect due to the reduced API agglomeration [73]. Here, the impact of different silicas and their two different amounts was examined on the dissolution of mAPAP, even though it is a readily dissolving drug. For each case, 200 mg, 12.7 mm tablets each having tensile strengths of about 2 MPa were selected and tested as discussed in Section 3.2.10. Tablet moisture content values and the relative surface wettability assessment using the sessile drop testing

were carried out to ensure that there were no appreciable differences amongst uncoated and four different silica coated formulations. The details of such testing are shown in *Supplementary Materials*, Section S1 and Fig. S2.

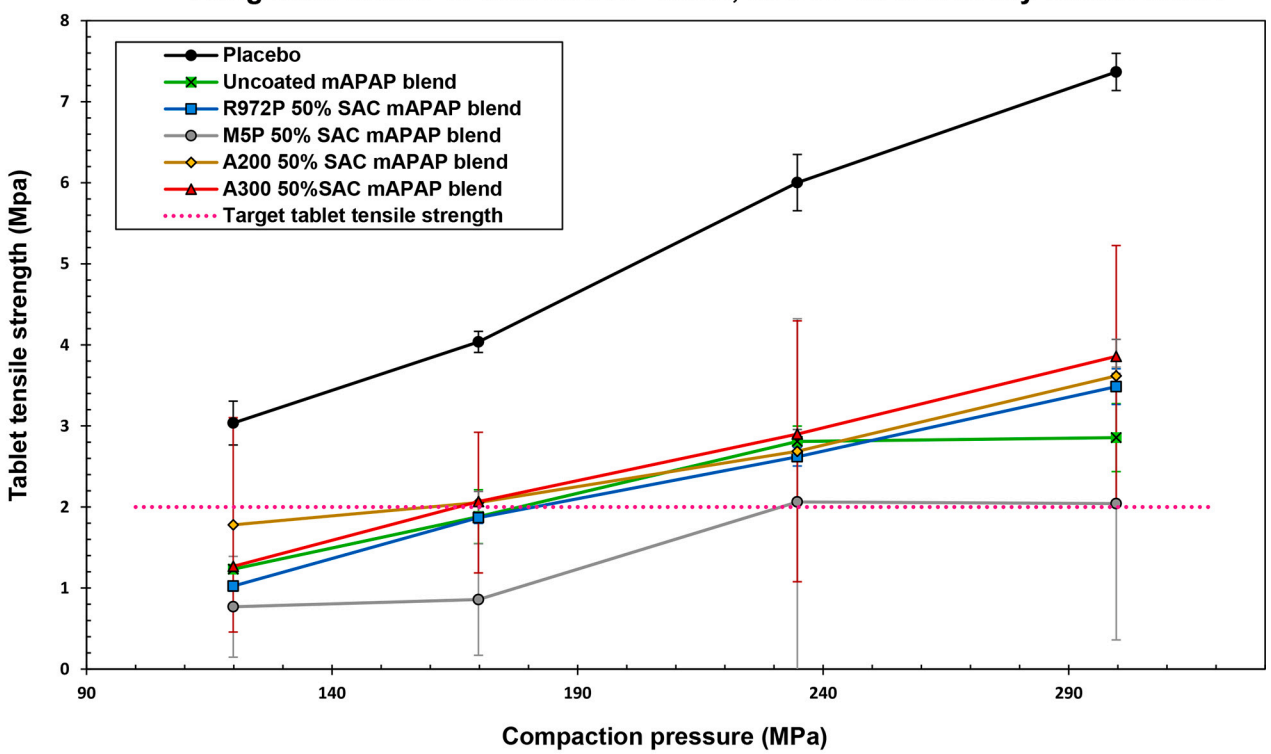
The mAPAP dissolution profiles are shown in Figs. 8(a) and 8(b) for 50% SAC and 100% SAC, respectively. The results from Fig. 8(a) clearly convey that using lesser silica amounts of 50% SAC is better since there was little or no adverse effect of any of the four silicas on drug dissolution. In fact, even hydrophobic silica may be used without any loss in dissolution rate as compared to either uncoated API or hydrophilic silica coated API blends. For the higher silica amounts of 100% SAC, the dissolution profiles for silica A200 or A300 dry coated mAPAP tablets were similar to those of the uncoated mAPAP tablets (Fig. 8(b)), all achieving 80 wt% API dissolution within 40 min. Not too surprisingly, there was a slight adverse impact for the hydrophobic silica R972P at 100% SAC. This small drop may be justified because of the rather high wt% amount of hydrophobic silica, i.e., 100% SAC being equivalent to 3 wt% of R972P silica. The dissolution rate for the tablets with mAPAP coated with silica M5P were marginally better and may also be due to the higher amount of hydrophilic silica M5P as compared to A200 and A300. Nonetheless, these results indicate that dry coating with any of these four silicas, preferably in lesser silica amounts, could lead to positive outcomes from both the tablet strength and dissolution perspectives.

5. Conclusion

The experimental results of the four APIs and four silicas at two different % SAC levels showed that appreciable yet differing extent of property enhancements may be achieved with dry coating of silica, generally in line with the Chen's model predictions. The improvements in the reduced agglomeration, enhanced flowability, and increased bulk density were significant for three out of four APIs, GF being an exception due to its macro-rough surface, in line with the previous reports [75,82]. Nonetheless, minor differences existed amongst the various dry coated silica and API combinations, which may be attributed to the combined effect of various factors evident from the presented models. The analysis of silica sizes in range 7-100 nm, based on Chen's model [13] and Zheng's stick-bounce model [76], indicated that silica size stands out as the major driver for these fine APIs having three main effects: (1) silica amount required at each % SAC, (2) reduction in cohesion, and, (3) tendency for silica aggregation on to the API surfaces. Whereas the finer silica size was a better choice with respect to the first two factors, it was not necessarily the best choice because of the higher aggregation tendency for smaller silicas. The additional factors included: the surface energy, for which the dispersive component may impact the bonding strength and hence tablet TS, the total surface energy may impact the coating effectiveness based on guest-host compatibility, and silica hydrophobicity, which may impact API dissolution. Interestingly, the surface energy had a secondary effect on the tablet tensile strength, most likely because only one of the constituents of the blend was dry coated [59,70]. Another potential reason could be the differences in the powder rearrangement during tablet pre-compaction because of the lower powder cohesion due to dry coating, a topic that would require further research. Similarly, the hydrophobicity of silica R972P also had a secondary impact, which was attributed to reduced API agglomeration, in line with a previous detailed investigation based on two hydrophobic APIs, ibuprofen and fenofibrate [75]. Lastly, the SEM images provided qualitative indication that the use of high-intensity coating device largely negated the guest-host compatibility issues. All things

(a)

70mg/6mm tablet: 40 wt% mAPAP blend, mAPAP 50% SAC dry coated cases





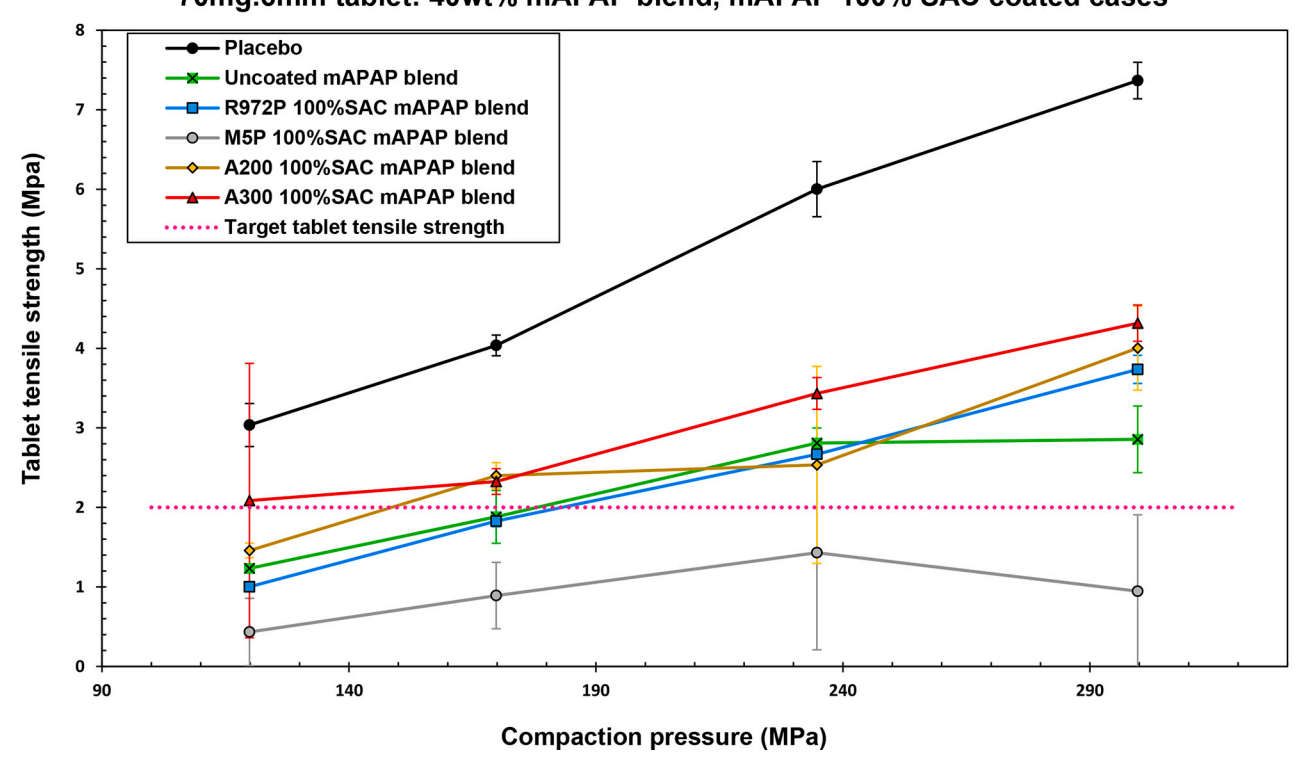
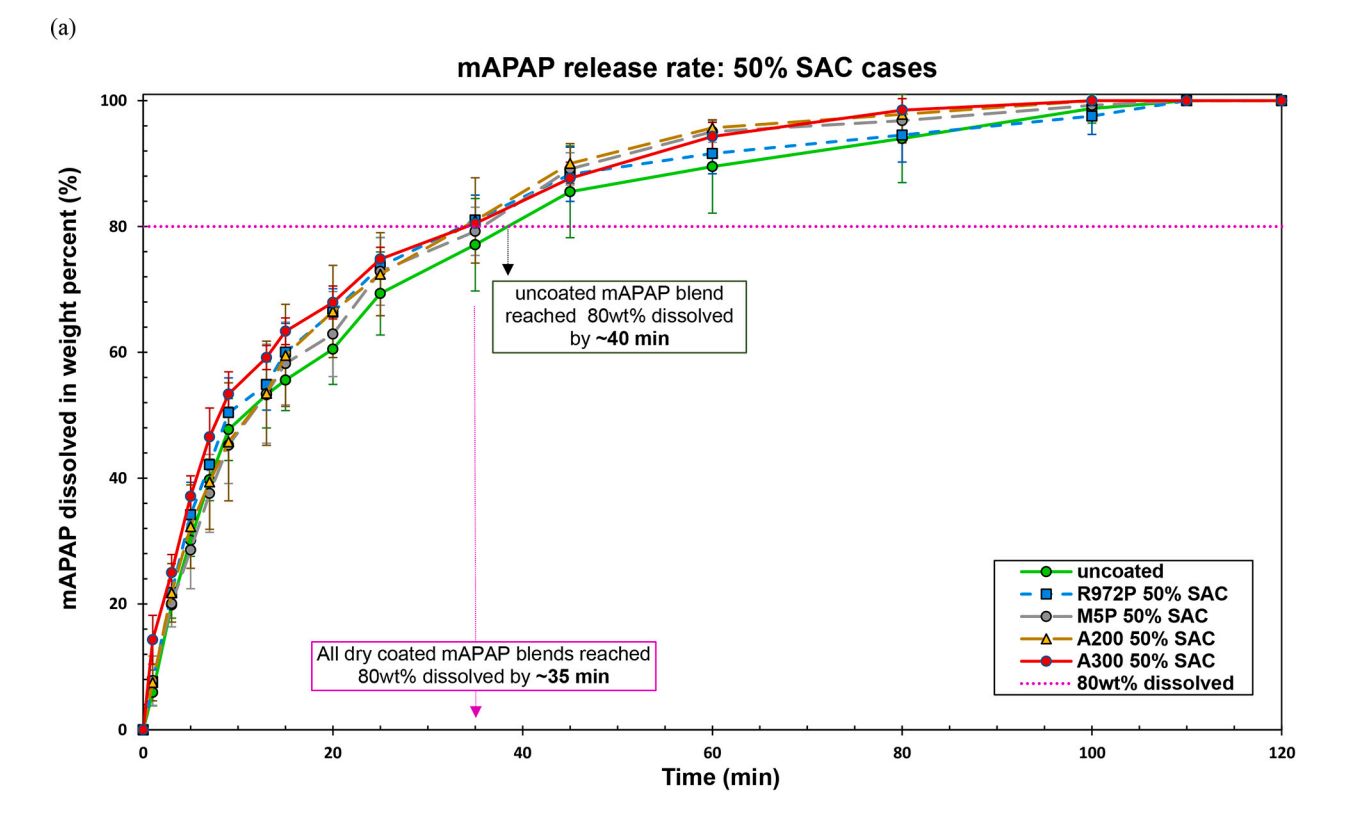


Fig. 7. Tablet tensile strength for blends with and without dry coating for different silica types as a function of the compaction pressure: (a) 50% SAC dry coating formulation cases, and (b) 100% SAC dry coating formulation cases. Ten tablets were tested per case to ensure reproducibility.

S.S. Kim et al. Powder Technology 432 (2024) 119104



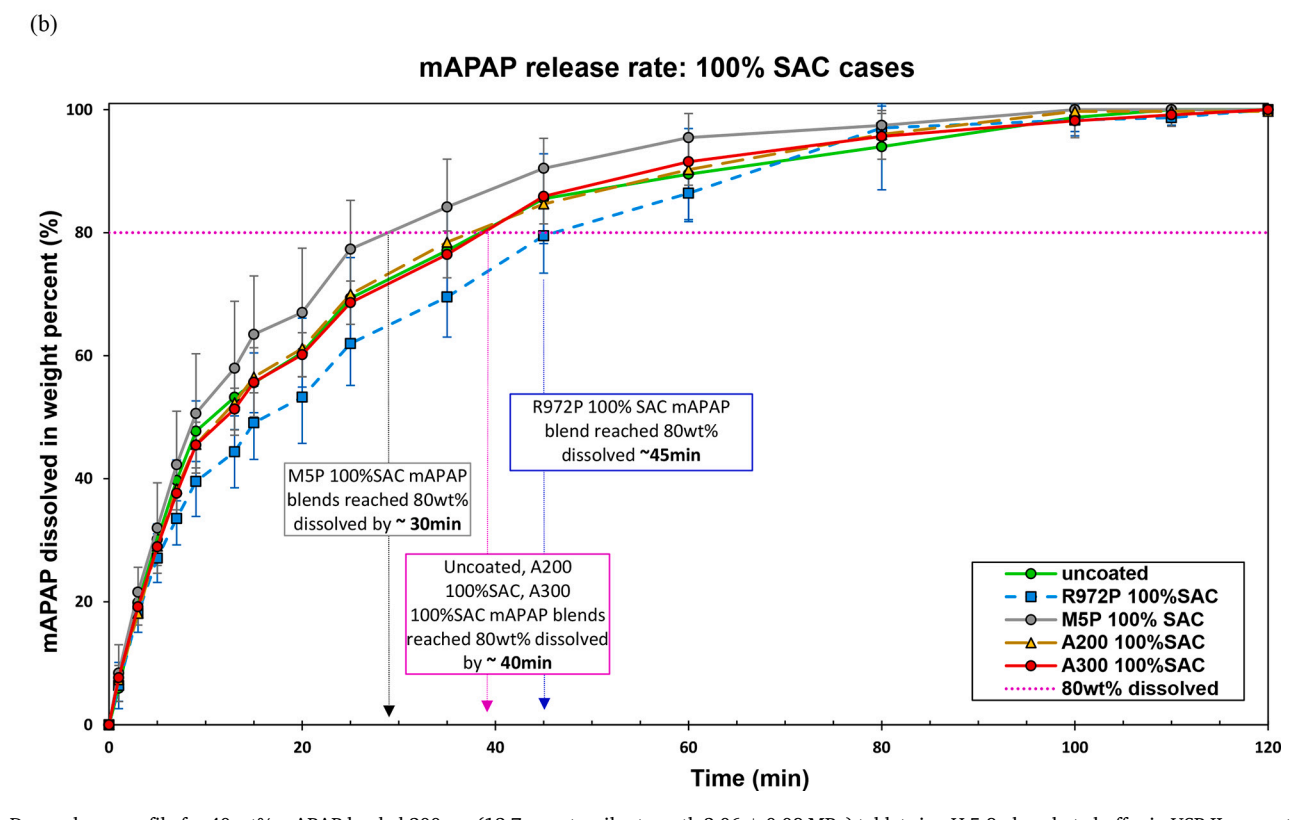


Fig. 8. Drug release profile for 40 wt% mAPAP loaded 200 mg (12.7 mm, tensile strength 2.06 ± 0.08 MPa) tablets in pH 5.8 phosphate buffer in USP II apparatus at 37.8 \pm 0.3 °C. 40 wt% of: (a) 50% SAC coated mAPAP blends, (b) 100% SAC coated mAPAP blends. Each test was repeated at least three times.

considered, the results demonstrated that the significant enhancements in flowability, bulk density, compactability, agglomeration reduction, and dissolution for API or blend may be achieved by dry coating with all silicas, although best overall outcomes were for R972P and A200 at

lower 50% SAC, corroborating with both the Chen and Deng models.

Funding sources

Financial support from National Science Foundation (NSF) grants IIP-1919037 (NSF-PFI-RP) and IIP-2137209 (NSF-IUCRC), along with the associated Industry Advisory Board (IAB) membership support to the Center for Materials Science and Engineering of Pharmaceutical Products (CIMSEPP), is gratefully acknowledged. The corresponding author is also grateful for the financial support from the International Fine Particle Research Institute (IFPRI).

CRediT authorship contribution statement

Sangah S. Kim: Conceptualization, Methodology, Validation, Formal analysis, Investigation, Data curation, Writing – original draft, Visualization, Supervision. Ameera Seetahal: Investigation. Christopher Kossor: Writing – review & editing. Rajesh N. Davé: Supervision, Conceptualization, Formal analysis, Data curation, Visualization, Resources, Funding acquisition, Writing – review & editing.

Declaration of Competing Interest

The authors declare that they have no known competing financial interests or personal relationships that could have appeared to influence the work reported in this paper.

Data availability

Data will be made available on request.

Acknowledgements

The authors thank Hadeel Darweesh, Chelsea Castillo, Mirna Cheikhali, Benjamin Marsiglia, and Nicholas Amores for assistance in sample preparation and testing. The authors are grateful for stimulating discussions with and suggestions from Dr. Chen Mao from *Genentech* and Dr. David Burnett from *Surface Measurement Systems* (SMS), during the CIMSEPP IAB meetings discussions. Special thanks also to Dr. David Burnett and Dr. Anett Kondor for their technical help in assessing the surface energy of the nano silica used in the current study. Generous donations and contributions of materials and characterization instruments are acknowledged from BASF, DFE Pharma, Evonik, Freeman Technology, FMC Biopolymer (now IFF), Gamlen, and Mallinckrodt.

Appendix A. Supplementary data

Supplementary data to this article can be found online at https://doi.org/10.1016/j.powtec.2023.119104.

References

- G.G. Liversidge, K.C. Cundy, Particle size reduction for improvement of oral bioavailability of hydrophobic drugs: I. Absolute oral bioavailability of nanocrystalline danazol in beagle dogs, Int. J. Pharm. 125 (1995) 91–97.
- [2] M. Vogt, K. Kunath, J.B. Dressman, Dissolution enhancement of fenofibrate by micronization, cogrinding and spray-drying: comparison with commercial preparations, Eur. J. Pharm. Biopharm. 68 (2008) 283–288.
- [3] J.T. Hargrove, W.S. Maxson, A.C. Wentz, Absorption of oral progesterone is influenced by vehicle and particle size, Am. J. Obstet. Gynecol. 161 (1989) 948–951.
- [4] E. Merisko-Liversidge, Nanosizing: "end-to-end" formulation strategy for poorly water-soluble molecules, in: Discovering and Developing Molecules with Optimal Drug-Like Properties, 2015, pp. 437–467.
- [5] J. Visser, Van der Waals and other cohesive forces affecting powder fluidization, Powder Technol. 58 (1989) 1–10.
- [6] H. Shi, R. Mohanty, S. Chakravarty, R. Cabiscol, M. Morgeneyer, H. Zetzener, J. Y. Ooi, A. Kwade, S. Luding, V. Magnanimo, Effect of particle size and cohesion on powder yielding and flow, KONA Powder Part J 35 (2018) 226–250.
- [7] J.M. Valverde, A. Castellanos, Compaction of fine powders: from fluidized agglomerates to primary particles, Granul. Matter 9 (2007) 19–24.
- [8] A. Castellanos, The relationship between attractive interparticle forces and bulk behaviour in dry and uncharged fine powders, Adv. Phys. 54 (2005) 263–376.

- [9] S.T. Nase, W.L. Vargas, A.A. Abatan, J.J. McCarthy, Discrete characterization tools for cohesive granular material, Powder Technol. 116 (2001) 214–223.
- [10] J.W. Carson, T.A. Royal, D.J. Goodwill, Understanding and eliminating particle segregation problems, Bulk Solids Handling 6 (1986) 139–144.
- [11] J. Yang, A. Sliva, A. Banerjee, R.N. Dave, R. Pfeffer, Dry particle coating for improving the flowability of cohesive powders, Powder Technol. 158 (2005) 21–33
- [12] J. Scicolone, A. Mujumdar, S. Sundaresan, R.N. Davé, Environmentally benign dry mechanical mixing of nano-particles using magnetically assisted impaction mixing process, Powder Technol. 209 (2011) 138–146.
- [13] Y. Chen, J. Yang, R.N. Dave, R. Pfeffer, Fluidization of coated group C powders, AICHE J. 54 (2008) 104–121.
- [14] R. Pfeffer, R.N. Dave, D. Wei, M. Ramlakhan, Synthesis of engineered particulates with tailored properties using dry particle coating, Powder Technol. 117 (2001) 40–67
- [15] M.J. Espin, J.M.P. Ebri, J.M. Valverde, Tensile strength and compressibility of fine CaCO3 powders. Effect of nanosilica addition, Chem. Eng. J. 378 (2019).
- [16] M. Koishi, H. Honda, T. Ishizaka, T. Matsuno, T. Katano, K. Ono, Surface modification of powders by the high speed impact treatment method, J. Soc Powder Technol. Japan 5 (1987).
- [17] Y. Ouabbas, A. Chamayou, L. Galet, M. Baron, G. Thomas, P. Grosseau, B. Guilhot, Surface modification of silica particles by dry coating: characterization and powder ageing, Powder Technol. 190 (2009) 200–209.
- [18] M.P. Mullarney, L.E. Beach, R.N. Davé, B.A. Langdon, M. Polizzi, D.O. Blackwood, Applying dry powder coatings to pharmaceutical powders using a comil for improving powder flow and bulk density, Powder Technol. 212 (2011) 397–402.
- [19] M.P. Mullarney, L.E. Beach, B.A. Langdon, M.A. Polizzi, Applying dry powder coatings: using a resonant acoustic mixer to improve powder flow and bulk density, Pharm. Technol. 35 (2011) 94–102.
- [20] M. Naito, T. Hotta, T. Fukui, Applications of comminution techniques for the surface design of powder materials, Key Eng. Mater. 253 (2003) 275–292.
- [21] T. Yokoyama, K. Urayama, M. Naito, M. Kato, T. Yokoyama, The Angmill Mechanofusion system and its applications, KONA Powder Part. J. 5 (1987) 50-68
- [22] H.Y. Xie, The role of interparticle forces in the fluidization of fine particles, Powder Technol. 94 (1997) 99–108.
- [23] K. Tanno, Current status of the mechanofusion process for producing composite particles, Kona Powder Part. J. 8 (1990) 74–82.
- [24] M. Koishi, T. Ishizaka, T. Nakajima, Preparation and surface properties of encapsulated powder pharmaceuticals, Appl. Biochem. Biotechnol. 10 (1984) 259-262
- [25] J. Koskela, D.A.V. Morton, P.J. Stewart, A.M. Juppo, S. Lakio, The effect of mechanical dry coating with magnesium stearate on flowability and compactibility of plastically deforming microcrystalline cellulose powders, Int. J. Pharm. 537 (2018) 64–72.
- [26] T. Ishizaka, K. Ikawa, N. Kizu, H. Honda, M. Koishi, K. Yano, Complexation of aspirin with potato starch and improvement of dissolution rate by dry mixing, Chem. Pharm. Bull. 36 (1988) 2562–2569.
- [27] M. Senna, Atomic processes during mechanical compounding with metal hydroxides, Mater. Sci. Forum 312 (1999) 167–172.
- [28] M. Senna, More chemistry for finer particle technology, Chem. Eng. Res. Des. 76 (1998) 767–774.
- [29] M. Alonso, A Fundamental Study on the Coating of Powders, University of Osaka Prefecture, Osaka, Japan, 1991.
- [30] H. Suzuki, M. Shimizu, H. Kamiya, T. Ota, M. Takahashi, Preparation of fine mullite powders with high surface area by agglomeration control of alkoxidederived precursor sol, Adv. Powder Technol. 8 (1997) 12.
- [31] S. Watano, Y. Imada, K. Miyanami, C.Y. Wu, R.N. Dave, R. Pfeffer, T. Yoshida, Surface modification of food fiber by dry particle coating, J. Chem. Eng. Jpn 33 (2000) 848–854
- [32] Y. Kawashima, T. Serigano, T. Hino, H. Yamamoto, H. Takeuchi, Design of inhalation dry powder of pranlukast hydrate to improve dispersibility by the surface modification with light anhydrous silicic acid (AEROSIL 200), Int. J. Pharm. 173 (1998) 243–251.
- [33] W. Hendrickson, R. Kooyer, Process for Making Particle-Coated Solid Substrates, USA, 2000.
- [34] S. Watano, R. Pfeffer, R. Dave, Method of Particle Coating, USA, 2001.
- [35] Q. Zhang, J. Yang, S. Teng, R.N. Dave, L. Zhu, P. Wang, M.W. Young, C.G. Gogos, In-situ, simultaneous milling and coating of particulates with nanoparticles, Powder Technol. 196 (2009) 292–297.
- [36] P. Wang, L. Zhu, S. Teng, Q. Zhang, M.W. Young, C. Gogos, A novel process for simultaneous milling and coating of particulates, Powder Technol. 193 (2009) 65–68.
- [37] H. Liu, C. Lu, S.H. Patel, L. Zhu, M.W. Young, C.G. Gogos, P.C. Bonnett, Simultaneous milling, coating and coat-curing of particulates in a fluid energy mill via photo-polymerization, in: Annual Technical Conference - ANTEC, Conference Proceedings, 2012, pp. 2137–2141.
- [38] S. Chattoraj, L. Shi, C.C. Sun, Profoundly improving flow properties of a cohesive cellulose powder by surface coating with nano-silica through comilling, J. Pharm. Sci. 100 (2011) 4943–4952.
- [39] M. Capece, C. Borchardt, A. Jayaraman, Improving the effectiveness of the Comil as a dry-coating process: enabling direct compaction for high drug loading formulations, Powder Technol. 379 (2021) 617–629.
- [40] A. Kottlan, B.J. Glasser, J.G. Khinast, Powder bed dynamics of a single-tablet-scale vibratory mixing process, Powder Technol. 414 (2023).

[41] J.G. Osorio, F.J. Muzzio, Evaluation of resonant acoustic mixing performance, Powder Technol. 278 (2015) 46–56.

S.S. Kim et al.

- [42] H. Honda, K. Ono, T. Ishizak, T. Matsuno, M. Katano, M. Koishi, Surface modification of powders by the high speed impact treatment method, J. Soc. Powder Technol. Japan 24 (1987) 6.
- [43] H. Honda, T. Matsuno, M. Koishi, The effect of powder properties on dry impact blending preparation method, J. Soc. Powder Technol. Japan 25 (1989) 5.
- [44] H. Honda, T. Matsuno, M. Koishi, Preparation of a graphite fluoride modified-polymer microsphere by a high speed impact treatment method, J. Soc. Powder Technol. Japan 25 (1988) 5.
- [45] J. Kujawa, S. Cerneaux, W. Kujawski, Characterization of the surface modification process of Al2O3, TiO2 and ZrO2 powders by PFAS molecules, Colloids Surf. A Physicochem. Eng. Asp. 447 (2014) 14–22.
- [46] T. Iwasaki, Evaluation of Mechanical Energy Applied to Powders in Dry Processes and its Application for Design and Preparation of Functional Particulate Materials, Powder Engineering, Technology and Applications, 2011, pp. 257–310.
- [47] M. Gera, V.A. Saharan, M. Kataria, V. Kukkar, Mechanical methods for dry particle coating processes and their applications in drug delivery and development, Recent Patents Drug Deliv. Formul. 4 (2010) 58–81.
- [48] F. Zhu, J. Zhang, Z. Yang, Y. Guo, H. Li, Y. Zhang, The dispersion study of TiO2 nanoparticles surface modified through plasma polymerization, Phys. E. 27 (2005) 457–461.
- [49] I. Zimmermann, M. Eber, K. Meyer, Nanomaterials as flow regulators in dry powders, Z. Phys. Chem. 218 (2004) 51–102.
- [50] K. Meyer, I. Zimmermann, Effect of glidants in binary powder mixtures, Powder Technol. 139 (2004) 40–54.
- [51] Q.T. Zhou, L. Qu, I. Larson, P.J. Stewart, D.A.V. Morton, Effect of mechanical dry particle coating on the improvement of powder flowability for lactose monohydrate: a model cohesive pharmaceutical powder, Powder Technol. 207 (2011) 414–421.
- [52] L. Qu, D.A.V. Morton, Q.T. Zhou, Particle engineering via mechanical dry coating in the design of pharmaceutical solid dosage forms, Curr. Pharm. Des. 21 (2015) 5802–5814
- [53] L. Qu, Q. Zhou, J.A. Denman, P.J. Stewart, K.P. Hapgood, D.A.V. Morton, Influence of coating material on the flowability and dissolution of dry-coated fine ibuprofen powders, Eur. J. Pharm. Sci. 78 (2015) 264–272.
- [54] K. Pingali, R. Mendez, D. Lewis, B. Michniak-Kohn, A. Cuitino, F. Muzzio, Mixing order of glidant and lubricant - influence on powder and tablet properties, Int. J. Pharm. 409 (2011) 269–277.
- [55] N.O. Sierra-Vega, A. Román-Ospino, J. Scicolone, F.J. Muzzio, R.J. Romañach, R. Méndez, Assessment of blend uniformity in a continuous tablet manufacturing process, Int. J. Pharm. 560 (2019) 322–333.
- [56] L. Li, S. Sun, T. Parumasivam, J.A. Denman, T. Gengenbach, P. Tang, S. Mao, H. K. Chan, L-leucine as an excipient against moisture on in vitro aerosolization performances of highly hygroscopic spray-dried powders, Eur. J. Pharm. Biopharm. 102 (2016) 132–141.
- [57] A.D. Brunaugh, H.D.C. Smyth, Formulation techniques for high dose dry powders, Int. J. Pharm. 547 (2018) 489–498.
- [58] R.N. Dave, S. Kim, K. Kunnath, S. Tripathi, A concise treatise on model-based enhancements of cohesive powder properties via dry particle coating, Adv. Powder Technol. 33 (2022).
- [59] L. Chen, X. Ding, Z. He, Z. Huang, K.T. Kunnath, K. Zheng, R.N. Davé, Surface engineered excipients: I. Improved functional properties of fine grade microcrystalline cellulose, Int. J. Pharm. 536 (2018) 127–137.
- [60] M. Capece, Z. Huang, R. Davé, Insight into a novel strategy for the Design of Tablet Formulations Intended for direct compression, J. Pharm. Sci. 106 (2017) 1608–1617
- [61] T. Kojima, J.A. Elliott, Effect of silica nanoparticles on the bulk flow properties of fine cohesive powders, Chem. Eng. Sci. 101 (2013) 315–328.
- [62] D. Sunkara, M. Capece, Influence of material properties on the effectiveness of Glidants used to improve the Flowability of cohesive pharmaceutical powders, AAPS PharmSciTech 19 (2018) 1920–1930.
- [63] K. Kunnath, Z. Huang, L. Chen, K. Zheng, R. Davé, Improved properties of fine active pharmaceutical ingredient powder blends and tablets at high drug loading via dry particle coating, Int. J. Pharm. 543 (2018) 288–299.
- [64] L.J. Jallo, R.N. Dave, Explaining electrostatic charging and flow of surface-modified acetaminophen powders as a function of relative humidity through surface energetics, J. Pharm. Sci. 104 (2015) 2225–2232.
- [65] S. Kim, E. Bilgili, R.N. Davé, Impact of altered hydrophobicity and reduced agglomeration on dissolution of micronized poorly water-soluble drug powders after dry coating, Int. J. Pharm. 606 (2021).
- [66] M.G. Cares Pacheco, M.C. Jiménez Garavito, A. Ober, F. Gerardin, E. Silvente, V. Falk, Effects of humidity and glidants on the flowability of pharmaceutical excipients. An experimental energetical approach during granular compaction, Int. J. Pharm. 604 (2021).
- [67] M. Ricaud, Technical risk prevention in the workplace, in: P. Houdy, M. Lahmani, F. Marano (Eds.), Nanoethics and Nanotoxicology, Springer Berlin Heidelberg, Berlin, Heidelberg, 2011, pp. 219–241.
- [68] U.S.F.D.A. FDA, Code of Federal Regulations Title 21, 2022.
- [69] X. Han, L. Jallo, D. To, C. Ghoroi, R. Davé, Passivation of high-surface-energy sites of milled ibuprofen crystals via dry coating for reduced cohesion and improved flowability, J. Pharm. Sci. 102 (2013) 2282–2296.
- [70] S.S. Kim, C. Castillo, M. Sayedahmed, R.N. Dave, Reduced fine API agglomeration after dry coating for enhanced blend uniformity and processability of low drug loaded blends, Pharm. Res. 39 (2022) 19.

- [71] X. Deng, R.N. Davé, Adhesion and friction of dry-coated nano-rough particles, Powder Technol. 314 (2017) 20–27.
- [72] Z. Huang, W. Xiong, K. Kunnath, S. Bhaumik, R.N. Davé, Improving blend content uniformity via dry particle coating of micronized drug powders, Eur. J. Pharm. Sci. 104 (2017) 344–355.
- [73] S.S. Kim, C. Castillo, M. Cheikhali, H. Darweesh, C. Kossor, R.N. Dave, Enhanced blend uniformity and flowability of low drug loaded fine API blends via dry coating: the effect of mixing time and excipient size, Int. J. Pharm. 635 (2023).
- [74] K.T. Kunnath, S. Tripathi, S.S. Kim, L. Chen, K. Zheng, R.N. Davé, Selection of silica type and amount for Flowability enhancements via dry coating: contact mechanics based predictive approach, Pharm. Res. (2023), https://doi.org/ 10.1007/s11095-023-03561-6.
- [75] S. Kim, C. Cheikhali, R.N. Dave, Decoding Fine API Agglomeration as a Key Indicator of Powder Flowability and Dissolution: Impact of Particle Engineering Pharmaceutical Research, 2022, p. 20.
- [76] K. Zheng, K. Kunnath, Z. Ling, L. Chen, R.N. Davé, Influence of guest and host particle sizes on dry coating effectiveness: when not to use high mixing intensity, Powder Technol. 366 (2020) 150–163.
- [77] L.J. Jallo, Y. Chen, J. Bowen, F. Etzler, R. Dave, Prediction of inter-particle adhesion force from surface energy and surface roughness, J. Adhes. Sci. Technol. 25 (2011) 367–384.
- [78] F.M. Etzler, J. Drelich, Atomic Force Microscopy for Characterization of Surfaces, Particles, and Their Interactions, Developments in Surface Contamination and Cleaning: Detection, Characterization, and Analysis of Contaminants, 2012, pp. 307–331.
- [79] A.M. Azevedo, D.M.F. Prazeres, J.M.S. Cabral, L.P. Fonseca, Stability of free and immobilised peroxidase in aqueous-organic solvents mixtures, J. Mol. Catal. B Enzym. 15 (2001) 147–153.
- [80] F.M. Etzler, T. Bramante, R. Deanne, S. Sienkiewicz, F.J. Chen, Tablet tensile strength: an adhesion science perspective, J. Adhes. Sci. Technol. 25 (2011) 501–519.
- [81] D.R. Williams, Particle engineering in pharmaceutical solids processing: surface energy considerations, Curr. Pharm. Des. 21 (2015) 2677–2694.
- [82] K. Kunnath, S. Tripathi, S.S. Kim, L. Chen, K. Zheng, R.N. Dave, Selection of Silica Type and Amount for Flowability Enhancements Via Dry Coating: Contact Mechanics Based Predictive Approach, Pharmaceutical Research, 2023. Under review.
- [83] H. Rumpf, Die Wissenschaft des Agglomerierens, Chem. Ing. Tech. 46 (1974) 1.
- [84] F. Fulchini, U. Zafar, C. Hare, M. Ghadiri, H. Tantawy, H. Ahmadian, M. Poletto, Relationship between surface area coverage of flow-aids and flowability of cohesive particles, Powder Technol. 322 (2017) 417–427.
- [85] M. Capece, Z. Huang, D. To, M. Aloia, C. Muchira, R.N. Davé, A.B. Yu, Prediction of porosity from particle scale interactions: surface modification of fine cohesive powders, Powder Technol. 254 (2014) 103–113.
- [86] V. Swaminathan, D.O. Kildsig, Effect of magnesium stearate on the content uniformity of active ingredient in pharmaceutical powder mixtures, AAPS PharmSciTech 3 (2002).
- [87] M. Capece, R. Ho, J. Strong, P. Gao, Prediction of powder flow performance using a multi-component granular bond number, Powder Technol. 286 (2015) 561–571.
- [88] K. Kunnath, L. Chen, K. Zheng, R.N. Davé, Assessing predictability of packing porosity and bulk density enhancements after dry coating of pharmaceutical powders, Powder Technol. 377 (2021) 709–722.
- [89] S. Wu, Polar and nonpolar interactions in adhesion, J. Adhes. 5 (1973) 39-55.
- [90] J. Chen, D. Krengel, D. Nishiura, M. Furuichi, H.G. Matuttis, A force-displacement relation based on the JKR theory for DEM simulations of adhesive particles, Powder Technol 427 (2023) 118742.
- [91] P. Patrício, The hertz contact in chain elastic collisions, Am. J. Phys. 72 (2004) 1488–1491.
- [92] X. Han, C. Ghoroi, D. To, Y. Chen, R. Davé, Simultaneous micronization and surface modification for improvement of flow and dissolution of drug particles, Int. J. Pharm. 415 (2011) 185–195.
- [93] M. Azad, J. Moreno, E. Bilgili, R. Davé, Fast dissolution of poorly water soluble drugs from fluidized bed coated nanocomposites: impact of carrier size, Int. J. Pharm. 513 (2016) 319–331.
- [94] D.J. Sen, J.G. Pate, Logarithimic partition coefficient comparison study and molecular weight of synthesized Prodrgus of ibuprofen, + paracetamol, diclofenac sodium + paracetamol and ibuprofen + diclofenac sodium, Am. J. Adv. Drug Deliv. 4 (2016) 4.
- [95] L. Chen, X. Ding, Z. He, S. Fan, K.T. Kunnath, K. Zheng, R.N. Davé, Surface engineered excipients: II. Simultaneous milling and dry coating for preparation of fine-grade microcrystalline cellulose with enhanced properties, Int. J. Pharm. 546 (2018) 125–136.
- [96] L. Chen, Z. He, K.T. Kunnath, S. Fan, Y. Wei, X. Ding, K. Zheng, R.N. Davé, Surface engineered excipients: III. Facilitating direct compaction tableting of binary blends containing fine cohesive poorly-compactable APIs, Int. J. Pharm. 557 (2019) 354–365.
- [97] S. Paul, C.C. Sun, The suitability of common compressibility equations for characterizing plasticity of diverse powders, Int. J. Pharm. 532 (2017) 124–130.
- [98] G. Vreeman, C.C. Sun, Mean yield pressure from the in-die Heckel analysis is a reliable plasticity parameter, Int. J. Pharm. X 3 (2021).
- [99] X. Han, C. Ghoroi, R. Davé, Dry coating of micronized API powders for improved dissolution of directly compacted tablets with high drug loading, Int. J. Pharm. 442 (2013) 74–85.

- [100] C. Allenspach, P. Timmins, S. Sharif, T. Minko, Characterization of a novel hydroxypropyl methylcellulose (HPMC) direct compression grade excipient for pharmaceutical tablets, Int. J. Pharm. 583 (2020).
- [101] A.G. Stavrou, C. Hare, A. Hassanpour, C.Y. Wu, Investigation of powder flowability at low stresses: influence of particle size and size distribution, Powder Technol. 364 (2020) 98–114.
- [102] A. Zakhvatayeva, W. Zhong, H.A. Makroo, C. Hare, C.Y. Wu, An experimental study of die filling of pharmaceutical powders using a rotary die filling system, Int. J. Pharm. 553 (2018) 84–96.
- [103] L. Zuo, S.D.N. Lourenco, B.A. Baudet, Experimental insight into the particle morphology changes associated with landslide movement, Landslides 16 (2019) 787–798
- [104] R. Freeman, Measuring the flow properties of consolidated, conditioned and aerated powders - a comparative study using a powder rheometer and a rotational shear cell, Powder Technol. 174 (2007) 25–33.
- [105] D. Schulze, J. Schwedes, J.W. Carson, Powders and Bulk Solids: Behavior, Characterization, Storage and Flow, 2008.
- [106] A. Alexander, T. Shinbrot, B. Johnson, F.J. Muzzio, V-blender segregation patterns for free-flowing materials: effects of blender capacity and fill level, Int. J. Pharm. 269 (2004) 19–28.
- [107] Powderprocess, Engineering resources for powder processing industries, Powder Mixing Engineering Guide, in: A Free Online Engineering Guide to the Mixing of Powder, Granules and more Generally Bulk Solids, 2017.
- [108] D.E. Axe, Factors affecting uniformity of a mix, Anim. Feed Sci. Technol. 53 (1995) 211–220.
- [109] P. Shenoy, M. Viau, K. Tammel, F. Innings, J. Fitzpatrick, L. Ahrné, Effect of powder densities, particle size and shape on mixture quality of binary food powder mixtures, Powder Technol. 272 (2015) 165–172.
- [110] G.K. Bolhuis, A.J. Smallenbroek, C.F. Lerk, Interaction of tablet disintegrants and magnesium stearate during mixing I: effect on tablet disintegration, J. Pharm. Sci. 70 (1981) 1328–1330.
- [111] A. Sauer, S. Warashina, S.M. Mishra, I. Lesser, K. Kirchhöfer, Downstream processing of spray-dried ASD with hypromellose acetate succinate – roller compaction and subsequent compression into high ASD load tablets, Int. J. Pharm. X 3 (2021).
- [112] L. Kalantzi, C. Reppas, J.B. Dressman, G.L. Amidon, H.E. Junginger, K.K. Midha, V.P. Shah, S.A. Stavchansky, D.M. Barends, Biowaiver monographs for immediate release solid oral dosage forms: acetaminophen (paracetamol), J. Pharm. Sci. 95 (2006) 4–14.
- [113] A. Alghunaim, S. Kirdponpattara, B.M.Z. Newby, Techniques for determining contact angle and wettability of powders, Powder Technol. 287 (2016) 201–215.
 [114] B. Yang, C. Wei, Y. Yang, Q. Wang, S. Li, Evaluation about wettability, water
- [114] B. Yang, C. Wei, Y. Yang, Q. Wang, S. Li, Evaluation about wettability, water absorption or swelling of excipients through various methods and the correlation between these parameters and tablet disintegration, Drug Dev. Ind. Pharm. 44 (2018) 1417–1425.
- [115] R.N. Dave, S. Kim, Z. Lin, Powder blend processability improvements through minimal amounts of synergistically selected surface coating agents, in: U.P. Office (Ed.), New Jersey Institute of Technology, USA, 2022.
- [116] A.M.N. Faqih, A. Mehrotra, S.V. Hammond, F.J. Muzzio, Effect of moisture and magnesium stearate concentration on flow properties of cohesive granular materials, Int. J. Pharm. 336 (2007) 338–345.
- [117] B.A.C. Carlin, Direct compression and the role of filler-binders, in: L. L. Ausgburger, S.W. Hoag (Eds.), Pharmaceutical Dosage Forms: Tablets, CRC Press, Boca Raton, 2008, p. 568.
- [118] A.K. Meena, D. Desai, A.T.M. Serajuddin, Development and optimization of a wet granulation process at elevated temperature for a poorly compactible drug using twin screw extruder for continuous manufacturing, J. Pharm. Sci. 106 (2017) 589-600
- [119] S.S. Kim, A. Seetahal, N. Amores, C. Kossor, R.N. Davé, Impact of Dry Coating and Mixing Time on Flowability and Drug Content Uniformity of Medium Drug Loaded Fine API Blends, Journal of Pharmaceutical Sciences, 2023. Under review.
- [120] Q. Zhou, L. Shi, S. Chattoraj, C.C. Sun, Preparation and characterization of surface-engineered coarse microcrystalline cellulose through dry coating with silica nanoparticles, J. Pharm. Sci. 101 (2012) 4258–4266.
- [121] C.C. Sun, Setting the bar for powder flow properties in successful high speed tableting, Powder Technol. 201 (2010) 106–108.
- [122] S.M. Razavi, J. Scicolone, R.D. Snee, A. Kumar, J. Bertels, P. Cappuyns, I. Van Assche, A.M. Cuitino, F. Muzzio, Prediction of tablet weight variability in continuous manufacturing, Int. J. Pharm. 575 (2020).
- [123] Y. Murase, K. Takayama, T. Uchimoto, H. Uchiyama, K. Kadota, Y. Tozuka, Prediction of tablet weight variability from bulk flow properties by sparse modeling, Powder Technol. 407 (2022).
- [124] USP-NF, <905> Uniformity of dosage units, in: FDA (Ed.), Stage 6 Harmonization, United States Pharmacopeia, 2011, p. 3.
- [125] C.C. Sun, H. Hou, P. Gao, C. Ma, C. Medina, F.J. Alvarez, Development of a high drug load tablet formulation based on assessment of powder manufacturability: moving towards quality by design, J. Pharm. Sci. 98 (2009) 239–247.

- [126] S. Dawoodbhai, C.T. Rhodes, The effect of moisture on powder flow and on compaction and physical stability of tablets, Drug Dev. Ind. Pharm. 15 (1989) 1577–1600.
- [127] C.C. Sun, Role of surface free energy in powder behavior and tablet strength, Adhesion Pharm. Biomed. Dent. Fields (2017) 75–88.
- [128] S.H. Jeong, Y. Takaishi, Y. Fu, K. Park, Material properties for making fast dissolving tablets by a compression method, J. Mater. Chem. 18 (2008) 2577, 2525



Sangah S. Kim recently received her Ph.D. in the Department of Chemical and Materials Engineering at the New Jersey Institute of Technology. Prior to her work in Dr. Davé's lab, Sangah received her Master's in Engineering and Bachelor's in Engineering in Chemical Engineering at the Cooper Union, Albert Nerken School of Engineering (New York, NY). After graduation, she worked as a Research and Development Engineer at Hanwha Chemical (Daejeon, South Korea) for 4 years within the Polysilicon R&D and Process Development Departments to develop next-generation productions and processes. Her research interests include particle engineering and particle agglomeration.



Ameera Seetahal earned her bachelor's degree in Chemical Engineering and a minor in Business recent at the New Jersey Institute of Technology in May 2023. Throughout her academic career, she has worked in research and development roles in the chemical and pharmaceutical industry. Her interests pertain to continuing research in pharmaceuticals and eventually obtaining a master's degree in Chemical Engineering.



Christopher Kossor is a Ph.D. candidate in the Department of Chemical and Materials Engineering at the New Jersey Institute of Technology. He received a Bachelor of Science in Chemical Engineering from the New Jersey Institute of Technology in May 2021 while interning in process development and commercialization roles within the pharmaceutical industry. After researching pharmaceutical applications of 3D printing in Dr. Davé's lab, he joined the lab full time upon graduation. His research interests include the processability of amorphous solid dispersions and particle engineering.



Rajesh Davé, Fellow of the American Institute of Chemical Engineers, American Association of Pharmaceutical Scientists, and National Academy of Inventors, is a Distinguished Professor of Chemical and Materials Engineering at NJIT. His research contributions include ~200 journal papers (14,900+ Google citations, H-Index 65), and 22 issued patents. He has granted 37 PhDs, seven as faculty in US. He has received numerous national awards, including, 2022 AIChE PD2M Award for Outstanding Contribution to QbD for Drug Product, 2016 Edison Patent Award, and 2015 AIChE Particle Technology Forum Fluidization Lectureship. He is currently the U.S. Executive Editor of Advanced Powder Technology.